The Dynamics of Circulations within the Trailing Stratiform Regions of Squall Lines. Part II: Influence of the Convective Line and Ambient Environment

WILLIAM A. GALLUS JR.* AND RICHARD H. JOHNSON

Department of Atmospheric Science, Colorado State University, Fort Collins, Colorado

(Manuscript received 24 April 1994, in final form 5 January 1995)

ABSTRACT

A dynamic version of the two-dimensional kinematic cloud model of Rutledge and Houze is used to study the individual roles of hydrometeor and heat advection from the convective line to the stratiform region of the 10–11 June 1985 PRE-STORM squall line. The design of the model allows for specified inputs of hydrometeors, heat, and water vapor from the convective line.

Convective heating alone generates significant ascent and condensate in the anvil; however, surface rainfall is scarce without the advection of hydrometeors from the convective line. Hydrometeor advection alone does not produce strong ascent in the anvil cloud, implying the important additive effects of both heat and hydrometeor advection in generating broad regions of significant stratiform rainfall.

The roles of individual microphysical processes within the stratiform region are examined, along with the sensitivity of stratiform region dynamics to postconvective region environmental conditions. Of the processes evaporation, melting, and sublimation—evaporation in mesoscale downdrafts is the most important affecting the intensity of circulations such as the rear-inflow jet and precipitation—followed by melting and then sublimation. Stability strongly controls vertical motion in the stratiform region. Greater instability increases in situ production of condensate, surface rainfall, and low-level drying within the mesoscale downdraft. The intensity of hydrometeor advection from convective elements significantly influences surface rain rates in the stratiform region. These findings suggest that natural variability arising from three-dimensional convective line structures and inhomogeneities in the environment can induce significant hydrometeor and flow perturbations (asymmetries) in the trailing stratiform regions of squall lines.

1. Introduction

Squall lines with trailing stratiform precipitation regions have been studied extensively using data from a number of relatively recent research programs (e.g., Zipser 1977; Ogura and Liou 1980; Johnson and Hamilton 1988). These studies have found broad and pronounced mesoscale circulations associated with the systems, including an ascending front-to-rear (FTR) jet and a descending rear-inflow jet (Smull and Houze 1985). Mesoscale ascent typically occurs above the melting level within the stratiform region, with mesoscale descent below this level. The intensity and behavior of these circulations can vary widely among different squall line systems (e.g., Smull and Houze 1987).

Part I of this study (Gallus and Johnson 1995; GJ95) discussed a simulation of the 10–11 June 1985 PRE-STORM (Preliminary Regional Experiment for STORM-Central) squall line using a two-dimensional cloud/mesoscale model with a detailed six class bulk microphysical scheme. The model was used to simulate only the stratiform region of the system. In general, the model reasonably simulated the evolution of circulations, and the growth and evolution of the stratiform rain region. Vertical motions intensified during the development of the stratiform rain region, and in situ production of condensate became increasingly important as the system evolved.

The initial conditions used in the simulation of the 10–11 June system (GJ95) were based upon soundings from the region immediately behind the system during its early stages. Although the squall line was highly two-dimensional, some minor variations existed in stability and humidity in the along-line direction within the stratiform region.

Knupp and Cotton (1987) found that the peak upward motion in the stratiform anvil cloud occurred around the midpoint of a stable layer, suggesting that the mesoscale updraft may be sensitive to the stability of the environment. One-dimensional cumulonimbus models (Ferrier and Houze 1989), along with aircraft data (Heymsfield and Hjemfelt 1984) imply that hydrometeor contents within convective cells of different

* Current affiliation: UCAR visiting scientist, National Meteorological Center, Camp Springs, Maryland.

Corresponding author address: Dr. William A. Gallus, Jr., World Weather Building, National Meteorological Center, 5200 Auth Road, Camp Springs, MD 20746.

cases can vary substantially. This can be seen by comparing the mixing ratios used in the kinematic model studies of Rutledge (1986) for a tropical case, and Rutledge and Houze (1987) for a midlatitude case. These studies raise questions as to what effect differences in stability or hydrometeor advection might have on the behavior and evolution of circulations and rainfall within the stratiform region.

Because humidity and temperature varied somewhat within the stratiform region of the 10–11 June system, and to improve understanding of the role of various environmental conditions on the behavior of circulations in the stratiform region, several sensitivity tests are performed with the two-dimensional model. These sensitivity tests are described briefly in Table 1. The role of hydrometeor advection alone is isolated in C2, and the role of convective heating alone is investigated in C3. Individual microphysical processes are examined in simulations C4 through C6. The effects of stability changes are shown in S1 and S2. Simulations S3 and S4 are run to investigate the effect of changes in hydrometeor content within the convective cells. Last, sensitivity to convective-line heating rates is examined.

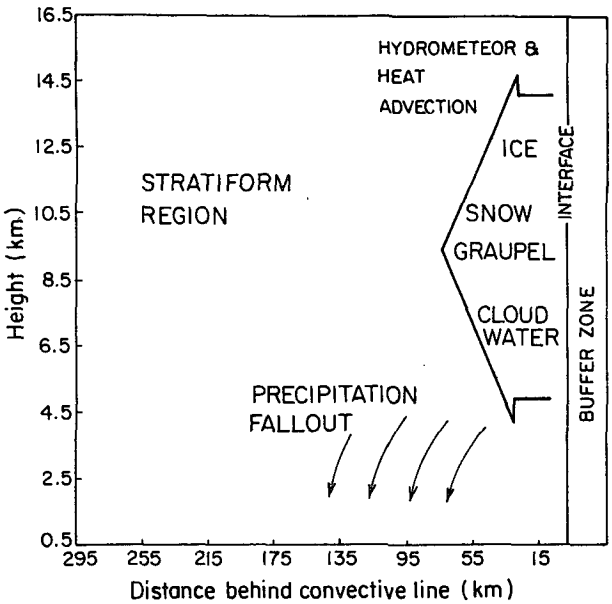

FIG. 1. Schematic of the model domain depicting important processes driving the circulations that may develop (from Gallus and Johnson 1995). Left edge of buffer zone at right of domain is assumed to be collocated with back edge of convective line region. Distance scale below the figure (and similar ones appearing later) refers to distance behind the back edge of the convective line region.

2. Description of the numerical model

As stated in Part I (GJ95), there are trade-offs associated with the numerical approach taken in this model—namely, to conduct an explicit simulation of the stratiform region only with externally specified inputs from the convective line. Although the difficult problem of simulating a realistic convective line is avoided, realistic representation of its effects on the stratiform region must be included. The convective line is assumed to influence the stratiform region, but the stratiform region cannot explicitly influence the convective line. As will be discussed below, this limitation may be mollified by assumptions regarding the convective inputs over the time period of integration.

The basic model equations and important numerical aspects are discussed in detail in Part I (GJ95). The bulk microphysical scheme of Rutledge and Hobbs (1983; 1984) with six classes of water substance (including three classes of ice) is used. For the simulations in this study, a uniformly spaced nonstaggered grid system with a 5 km Δx and 400 m Δz is used. The domain extends roughly 300 km in x and 16 km in z. Open radiative lateral boundaries are used (Orlanski 1976) with a rigid top and bottom.

The domain is assumed to travel with the convective system so that the right boundary of the inner domain always stays at the interface between the convective line and stratiform regions (Fig. 1). The model is driven by rearward transport of heat and hydrometeors from the convective line. Hydrometeor contents within

TABLE 1. List of simulations. A brief description of the purpose of each run is shown. The control run includes full microphysics, convective heating, and hydrometeor advection from convective cells.

Group	Simulation	Description
Full Microphysics	CTL	Control run for 11 June
	C2	Convective heating neglected from CTL
	C3	Hydrometeor advection from convective cells neglected from CTL
Role of individual processes	C4	Melting (cooling) neglected from CTL
	C5	Evaporation (cooling) neglected from CTL
	C6	Sublimation (cooling) neglected from CTL
Changes in environmental conditions	S1	Increased instability for initialization
	S2	Decreased instability for initialization
	S3	50% reduction in convective hydrometeor input
	S4	50% increase in convective hydrometeor input
	S5	Altered vertical profile of convective heating

the convective cells (Fig. 2a) are based on output from the 1D cumulonimbus model of Ferrier and Houze (1989), applied to this case by Rickenbach (1990). The vertical profiles include both hydrometeors detrained from the model, and condensate within the convective cells. A 20-km-wide "buffer" zone is used at the right boundary (Fig. 1) to smooth slightly the effects of microphysical processes near the boundary. Within this zone of five grid points, microphysical rates decrease linearly toward the outer boundary, and hydrometeors pass through the region without falling. In simulations that allow convective heating, the heating rate is prescribed in the buffer zone (Fig. 2b) with values roughly based on the heat budget of this case at 0300 UTC (Gallus and Johnson 1991). Because that study used rawinsonde data with a roughly 80 km resolution, and the convective heating in the model is prescribed over a 15-km-wide region, the idealized profile is taken from the zone of greatest heating in the 0300 UTC budget. In this zone, enhanced vertical gradients existed just below and above 6 km. The convective inputs are assumed to vary in a pulse-like manner over 30-min periods. As discussed in GJ95, the pulsing is supported by other studies and results in better agreement of the advected water mass with observations. In addition, the convective inputs are prescribed to grad-

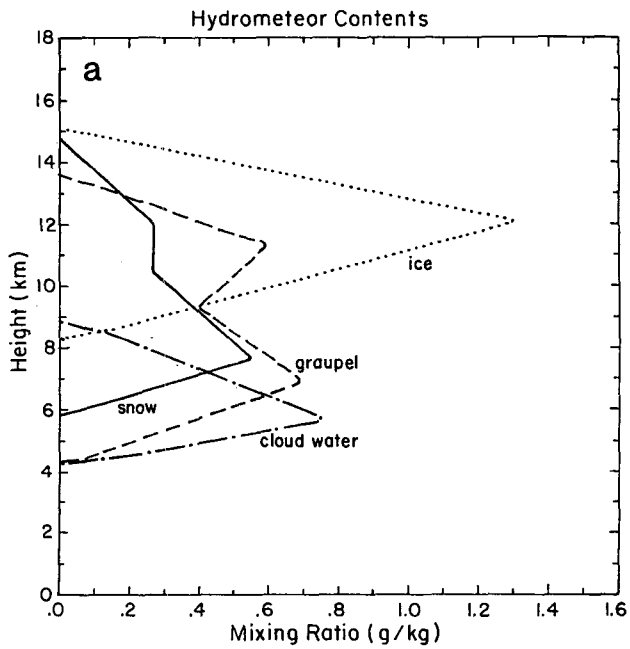

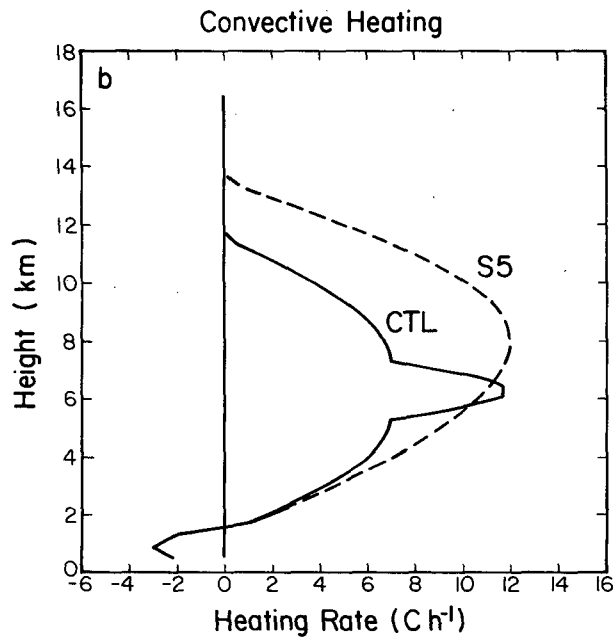

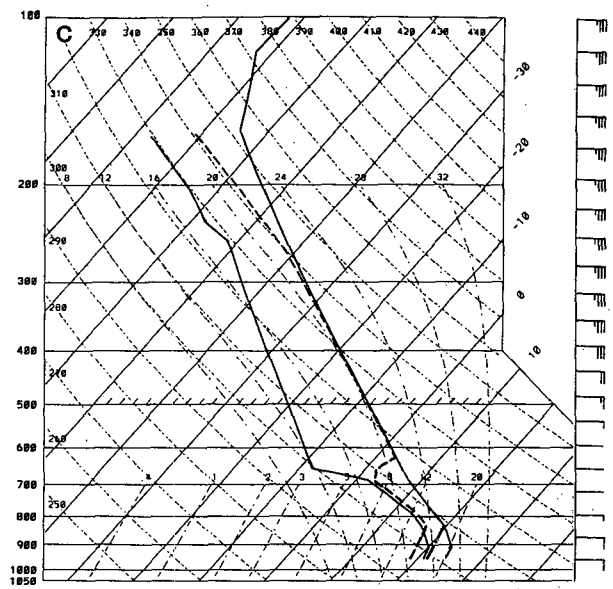

FIG. 2. Initial conditions used in simulations. Hydrometeor contents within convective cells shown in (a) with profiles of snow (solid), graupel (dashed), and cloud ice (dotted) averaged from Rickenbach (1990). Cloud water (dash–dotted) taken from Rutledge and Houze (1987). Convective heating profiles shown in (b) with CTL values (solid) taken from Gallus and Johnson (1991), and S5 values dashed. (c) Thermodynamic diagrams are shown with left boundary values solid and right boundary values dashed. Ambient wind is horizontally homogeneous and shown at right, with full barb = 5 m s^{-1}, half barb = 2.5 m s^{-1}.

ually decrease later in the simulations in agreement with observations that showed the convective elements weakening markedly after 0300 UTC. Because the stratiform region began to appreciably broaden around 0000 UTC 11 June, the initial model time can be thought of as corresponding to 0000 UTC. Prescribed hydrometeor contents begin to decrease at 300 min, ceasing at 405 min; convective heating decreases after 190 min, and is assumed negligible after 300 min. These temporal variations assume that hydrometeors continue advecting rearward from dissipating cells that have negligible diabatic heating for a period of time. Simulations are run to 420 min.

The initial wind field and thermodynamics are averaged from soundings that ascended in the front part of the 10–11 June system stratiform region as early in its lifetime as possible, with some modification based on the modeling study of Zhang and Gao (1989) and the Doppler radar study of Rutledge et al. (1988). The wind profile qualitatively resembles a mix between that of the presquall environment and the developing convective line region (see Figs. 2, 13; Gallus and Johnson 1992). Initially, FTR flow occurs at all levels with a distinct minimum around 4 km (Fig. 2c). Peak FTR flow near the surface is 6 m s^{-1}, and 17.5 m s^{-1} aloft. The flow is horizontally homogeneous with no vertical motion. Flow near the surface is slightly less than observed, partly because the free slip boundary condition required the vertical gradient to vanish in the lowest layer. The simulations are not sensitive to small changes in the velocity at this low level. The temperature field is generally horizontally homogeneous, but a 3 K cold pool is initialized in the lowest kilometer in the 75 km nearest the right boundary, to represent the region influenced by cold downdrafts from the newly developed convective line. Thermodynamic profiles from each lateral boundary are shown in Fig. 2c. Relative humidities decrease rearward from the convective line. Simulations C2–C6 use the same initial conditions as in CTL.

Because small thermodynamic variations existed in the along-line direction, sensitivity tests were done to investigate the response of the circulations to changes in the initial conditions that might fall within the range of observations. The circulations were not especially sensitive to variations in the initial humidity field, since the advection of water vapor from the convective line plays a dominant role. As will be discussed in section 7, more significant changes occur when stability is varied, along with the hydrometeor contents of the convective cells and the heating within them. However, the circulations are qualitatively not sensitive to reasonable changes in the initial conditions.

In simulations S1–S5, the initial conditions are the same as in CTL, except for variations in the one initial condition of interest. In simulations S1 and S2, stability is varied, but changes are kept reasonably small so that the lapse rates still agree reasonably well with observations. In S3 and S4, the solid hydrometeor mixing ratios are varied by 50%. In S5, the vertical profile of the convective heating is changed, but the peak magnitude remains the same as in CTL.

Realistically, changes in these individual parameters would not be independent. A change in the lapse rate of the environment would affect the strength of convective elements, in turn changing the amount of heating and hydrometeor advection. For simplicity, the sensitivity tests restrict the variations to one parameter. The primary purpose of the tests is to investigate what effect uncertainties in the initial conditions have on the circulations. However, the tests may also provide possible explanations for the differing behavior of stratiform regions among different cases, or explain variations in the along-line direction within a specific system. Because feedback from the stratiform region to the convective line cannot be simulated in the model, the results must be interpreted with an understanding of the specific behavior of the convective line assumed for this case. The reduction in convective inputs at later times in the simulations crudely represents one of the effects the stratiform region would have on the convective line, namely, the weakening of convection as the rear inflow jet strengthens the cold pool, leading to an eventual vorticity imbalance between the cold pool and ambient low-level shear (Rotunno et al. 1988).

3. CTL simulation

As discussed in detail in GJ95, the control run (CTL), which allows both hydrometeor and heat advection from the convective line, reasonably simulates the 10–11 June PRE-STORM system, particularly the evolution of the rain region and the behavior of the circulations. Surface rain rates increase with time and the rain region spreads rearward with a growing transition zone near the convective line (Fig. 3). The simulated rain area corresponds well with the observed region (averaged over the length of the system), shown with a bar at the base of each figure, but rain rates are underestimated.

The diabatic heating from microphysical processes within the stratiform region along with convective inputs produces an expanding area of positively buoyant air, generally above the melting level (Fig. 4). Perturbation buoyancies are defined as in Weisman (1992):

$$B = g\left(\frac{\theta}{\bar{\theta}} + 0.61(q_v - \bar{q}_v) - q_c - q_r\right),$$

where B represents the perturbation buoyancy, θ is the potential temperature, and q_v, q_c, and q_r are the mixing ratios of water vapor, cloud water, and rain, respectively. The 2D horizontal vorticity equation

$$\frac{d\eta}{dt} = \frac{\partial B}{\partial x},$$

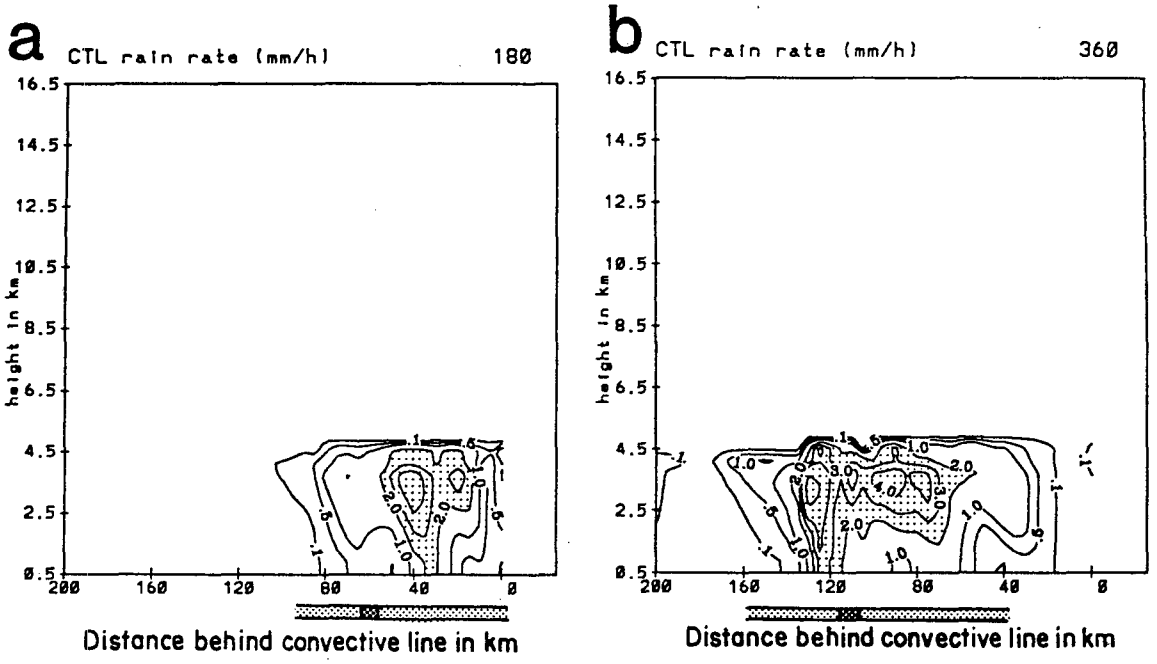

FIG. 3. Rain rates (in mm h^{-1}) at (a) 180 and (b) 360 min for the control run, CTL. Contour intervals of 0.1, 0.5, 1, 2, 3, 4, 6, and 8 mm h^{-1}, with rain rates greater than 2 mm h^{-1} shaded. The area of observed rain (averaged over the along-line direction) corresponding to the simulation times is shown with a bar below each figure. Enhanced rainfall is shown with darker stippling.

where $\eta = \partial u/\partial z - \partial w/\partial x$ shows that horizontal vorticity is generated by horizontal gradients of buoyancy. A significant horizontal gradient exists in midlevels, forcing the rear-inflow jet (Weisman 1992). Horizontal buoyancy gradients imply horizontal pressure gradients, and in this case, mesolows beneath the positively

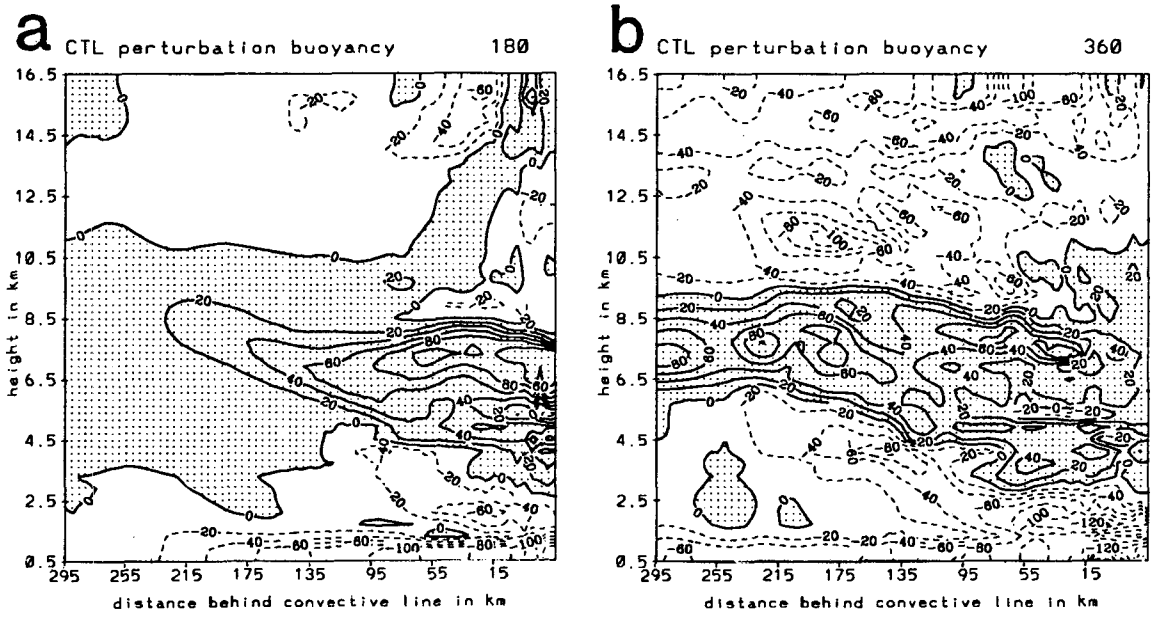

FIG. 4. Perturbation buoyancy fields (defined in text) at (a) 180 and (b) 360 min in CTL. Contour interval is 20×10^{-3} m s^{-2}, with positive perturbations shaded, and negative values dashed.

buoyant air aloft resulted in a pressure gradient force consistent with the formation of a rear-inflow jet (Gao et al. 1990). The buoyancy gradient is largest behind the main region of microphysical heating aloft and just ahead of the greatest microphysical cooling at low and middle levels. The greatest forcing advances rearward with time. Negative buoyancy is greatest in both the surface layer (due to the initial convectively produced cold bubble) and in the region near the sloping rear-inflow jet. Negative buoyancy above the 9–10-km level is primarily associated with cooling near the top of the mesoscale updraft. The rearward shift with time of the maximum positive buoyancy, and the peak magnitudes are in reasonable agreement with Weisman's (1992) moderate-shear simulation.

Upward motion develops in the anvil cloud, and although restricted to a small region just behind the convection at 180 min (Fig. 5a), ascent later occupies a 150-km area with maximum upward motion in the 7–10-km layer at 360 min (Fig. 5b). The cellular nature of the strongest ascent is due in part to the pulsing of the convective inputs, although a sensitivity test with constant convective inputs also evidenced somewhat similar features. During this time, rear-to-front (RTF) flow intensifies and expands rearward from the convective line at low levels, while FTR flow aloft also increases (Fig. 6). The total flow is the sum of the perturbations shown in Fig. 6 and the initial wind (Fig. 2c), and an example of this flow is shown at 360 min (Fig. 7). This total storm-relative flow agrees well with observations; FTR flow occurs near the surface and above the melting level with RTF flow confined to the rear-inflow jet extending from near the melting level 100–200 km from the convective line to the surface near the convection. (If the stronger observed wind was used in the lowest model layer instead of the ambient wind in Fig. 2c, FTR total storm-relative flow would be a few m s^{-1} stronger away from the convective line near the surface, and the rear-inflow jet would not quite reach the surface near the convective line.) The RTF perturbation flow at very high levels near the convective line implies that the initial strong FTR flow weakens there. The RTF flow is evidence of divergence from the top of the mesoscale updraft. Because the model does not explicitly simulate the convective line, the model may fail to show the full intensity of FTR flow here, which would be driven by divergence from the tops of the intense convective cells.

Qualitatively, the circulations resemble those observed (e.g., Rutledge et al. 1988), but upward motion is weaker above 9 km than observed, and the simulated rear-inflow jet is restricted to the 100 km or so region closest to the convective line, as opposed to the observed jet that was strong several hundred kilometers to the rear of the convection. The lack of radiative effects and the neglect of large-scale baroclinicity in the model are believed to contribute to these differences.

4. Hydrometeor advection alone

To investigate the effects of microphysical processes within the stratiform region acting on hydrometeors alone advected into the domain, simulation C2 is run without convective heating. In C2, it is assumed that

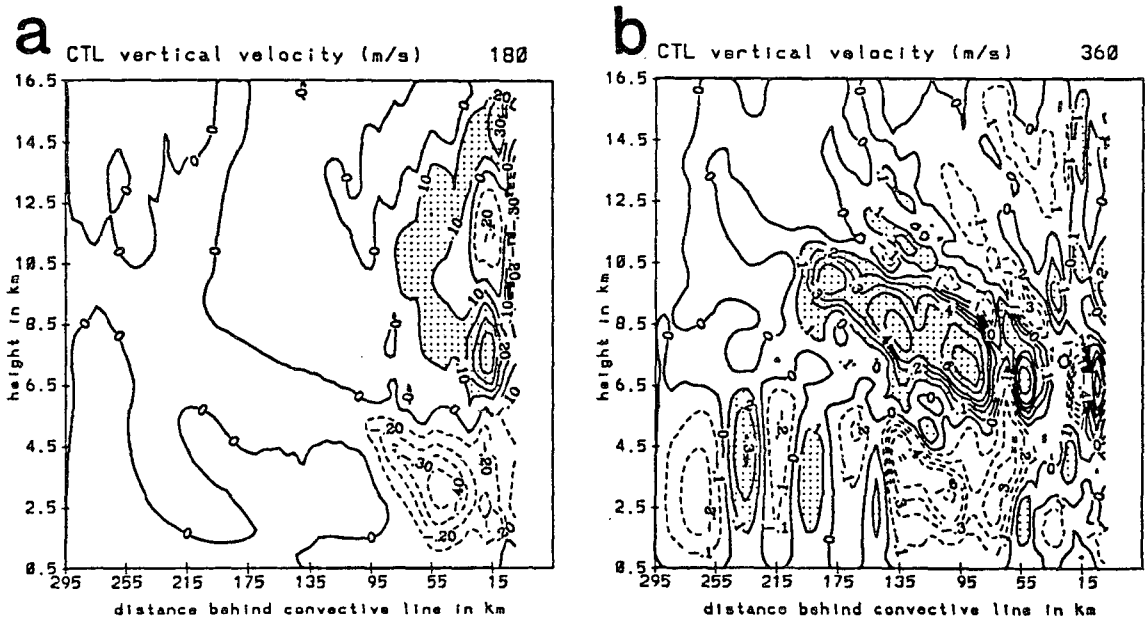

FIG. 5. Vertical velocities (in m s^{-1}) at (a) 180 and (b) 360 min for CTL. Contour interval is 0.1 m s^{-1} for absolute values less than 0.4 m s^{-1} and 0.2 m s^{-1} for larger values. Downward motion dashed and ascent greater than 0.1 m s^{-1} shaded.

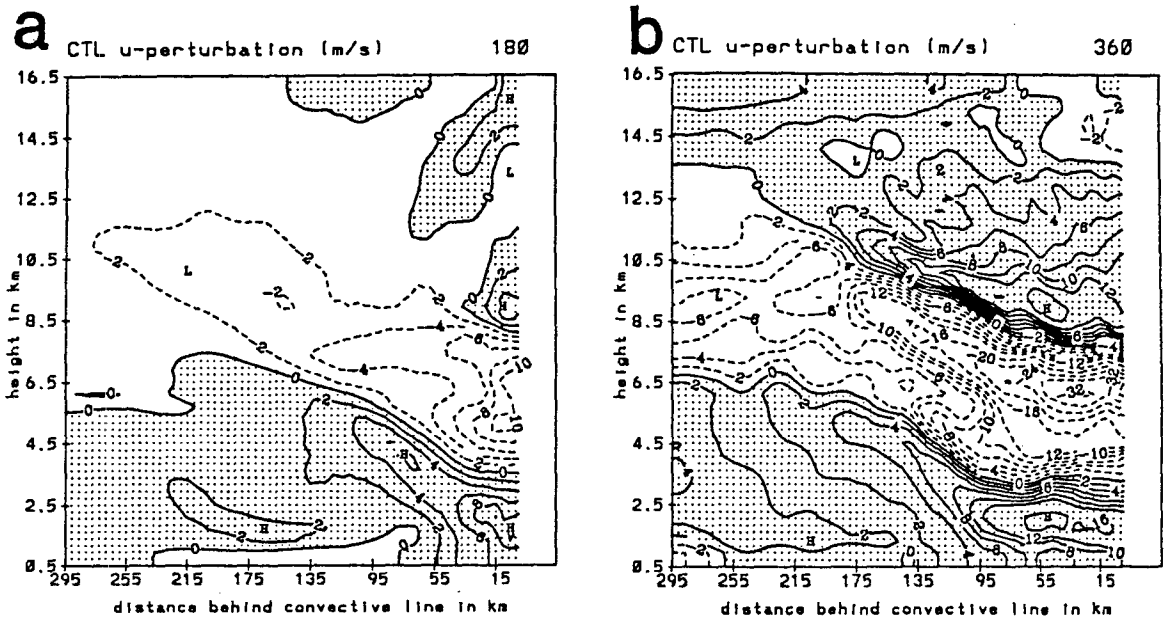

FIG. 6. Perturbation storm-relative u velocities (change in u in m s^{-1} since t_0) at (a) 180 and (b) 360 min for CTL. Front-to-rear flow is dashed and rear-to-front flow is shaded. Contour interval is 2 m s^{-1} for absolute values less than 12 m s^{-1}, and 4 m s^{-1} for larger values. Total storm-relative flow consists of the perturbation values added to the initial winds.

the only influence of the convective line after establishing FTR flow into the stratiform region is to supply hydrometeors to that area. Many observed features are simulated with good qualitative agreement to observations, as in CTL, but the magnitudes of the circulations are significantly less than those in CTL, which included effects from convective heating.

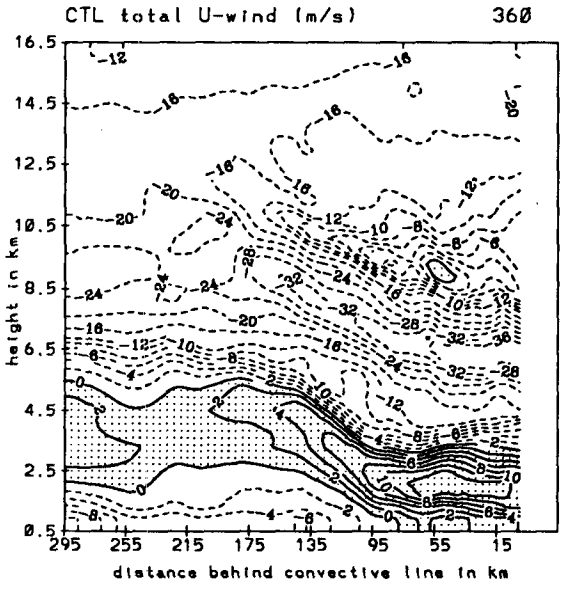

FIG. 7. Total storm-relative flow in m s^{-1} (ambient + perturbation) at 360 min for CTL. Front-to-rear flow is dashed and rear-to-front flow is shaded. Contour interval is 2 m s^{-1} for absolute values less than 12 m s^{-1}, and 4 m s^{-1} for larger values.

Snow, ice, and graupel mixing ratios are reduced roughly 10%–20% in C2 from CTL due to weaker ascent and a decrease in vapor deposition and condensation, and the decreases are reflected in diminished surface rainfall (Fig. 8) in C2 from that which occurred in CTL (Fig. 3). Peak surface rain rates are only around 1.5 mm h^{-1} in this simulation, half of what they were in CTL, and the peak values occur early, prior to 180 min (Fig. 8a). The area of surface rainfall does move rearward during the first 180 min, but rearward progression ceases after this time and measurable rain does not occur rearward of 95 km. In CTL, rainfall eventually reaches the surface 150 km to the rear of the convective line. The transition zone, or region of light rainfall just behind the convective line, is only around 15 km wide through most of the simulation and does not broaden significantly until late in the run.

In general, evaporation, melting, sublimation, deposition and condensation rates are all diminished in C2 from their values in CTL, resulting in a decrease in all terms of the integrated water budget (Table 2). This budget shows the liquid and solid water mass advected into the domain, created in situ through condensation and deposition, converted to vapor through the processes of evaporation and sublimation (mass sink), and reaching the surface (rain sink). The total amount of condensate produced in situ in C2 is only around 37% of that in CTL. A more detailed water budget (not shown) indicates that deposition is an order of mag-

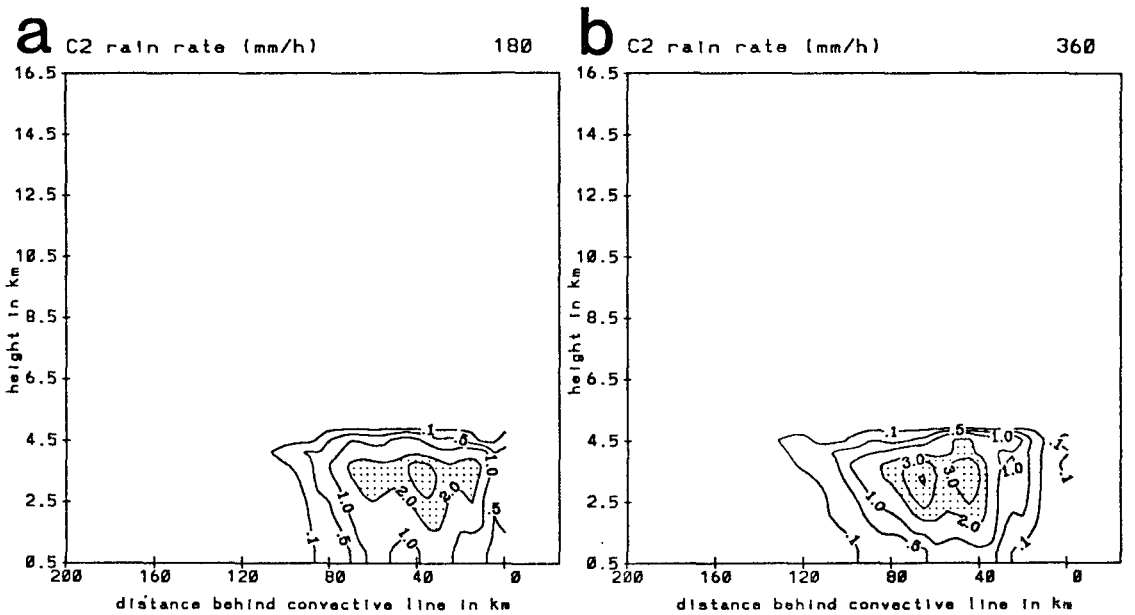

FIG. 8. As in Fig. 3 except for C2, the simulation excluding convective line heating.

nitude larger than condensation prior to 270 min, and still twice as large at later times. The decreased in situ production results in a 41% decrease in surface rainfall. The amount of condensate entering the domain from the convective line also decreases slightly, due to a weaker circulation than in CTL (Fig. 11).

The significant decrease in surface rainfall in this simulation is similar to the results in a sensitivity test performed with the kinematic model of Rutledge and Houze (1987), where hydrometeor advection continued, but vertical motion was ignored in the stratiform region. In that simulation, surface rainfall was only 25% that of the CTL run. The Rutledge and Houze result along with the results in C2 imply that although hydrometeor advection from the convective line is significant, much of the stratiform rainfall must be due to in situ condensate production. Precipitation efficiencies in C2 are comparable to those in CTL, since the weaker circulations reduce evaporation and sublimation.

Perturbation buoyancies are significantly diminished in C2 (Fig. 9) from CTL (Fig. 4). Without convective heating, horizontal buoyancy gradients are very weak near the convective line region. At 180 min (Fig. 9a), the negative buoyancy at low levels differs little from CTL, but by 360 min (Fig. 9b) the reduction in precipitation and resulting decrease in evaporation, melting, and sublimation results in much weaker negative buoyancies, particularly at distances greater than 100 km from the convective region.

Vertical motions throughout the domain in C2 (Fig. 10) are diminished from the CTL run (Fig. 5), but the most significant weakening is in the mesoscale updraft. At 180 min (Fig. 10a) ascent is only on the order of a few cm s^{-1}. Upward motion does not exceed 20 cm s^{-1} until 270 min, and peak values do not exceed 30 cm s^{-1} until 360 min (Fig. 10b). Upward motion in CTL exceeded 40 cm s^{-1} at 180 min and approached 1 m s^{-1} at 360 min.

The mesoscale downdraft, although diminished by 30% or so in strength, is again rather broad and well-organized. Peak values exceed 30 cm s^{-1} by 180 min (Fig. 10a) and eventually grow to nearly 45 cm s^{-1} at 360 min (Fig. 10b). The downdraft expands rearward with time as in CTL, but is 40 km less broad at 360 min, a reduction in size similar to that of the rain region (Fig. 8b). Heating within the convective line significantly affects the mesoscale ascent in the anvil cloud, but has a less significant, indirect effect on the mesoscale downdraft. The downdraft is more a function of processes within the stratiform precipitation region. The strong relationship between the scale of the mesoscale downdraft and the stratiform rain region has also been noted by Biggerstaff and Houze (1991).

Horizontal velocity perturbations are also diminished in C2 (Fig. 11) from CTL (Fig. 6). Perhaps the most important difference is that the rear-inflow perturbation near the back edge of the heaviest stratiform precipitation is nearly as strong as that at the front of the stratiform region during the first half of the simulation. By 180 min (Fig. 11a) rear inflow exceeds 5 m s^{-1} just below the melting level 80 km behind the convective line. This secondary peak in rear inflow remains relatively constant in magnitude and location near the back edge of the surface rain region throughout much of the remainder of the simulation. Prior to 270 min, the rear inflow in this region is nearly as strong

TABLE 2. Simplified integrated water budget of the CTL model simulation and simulations used in sensitivity tests. Values are in metric tons of water over the entire 405-min simulation, with percentage change from CTL run also shown. No convective heating in simulation C2, and no hydrometeor advection in simulation C3. In C4, melting is excluded from diabatic heating term, in C5 evaporation is excluded, and in C6, sublimation is excluded. Stability varies in S1 (more unstable) and S2 (more stable). Hydrometeor contents vary in S3 (50% less) and S4 (50% more). Convective heating profile changed in S5.

Run	Advected mass	In situ mass	Mass sink	Rain sink
CTL	1692.06	1246.98	2285.17	511.98
C2	1475.27 (−13%)	455.19 (−63%)	1458.02 (−36%)	300.42 (−41%)
C3	84.97 (−95%)	573.74 (−54%)	674.01 (−71%)	17.94 (−96%)
C4	1627.14 (−4%)	1028.73 (−18%)	1971.92 (−14%)	436.09 (−15%)
C5	1603.57 (−5%)	1193.17 (−4%)	1734.24 (−24%)	783.05 (+53%)
C6	1609.83 (−5%)	1235.19 (−1%)	2149.04 (−6%)	571.82 (+12%)
S1	1750.45 (+3%)	2256.36 (+81%)	3039.52 (+33%)	815.69 (+59%)
S2	1686.28 (−0%)	936.30 (−33%)	1839.25 (−19%)	595.18 (+16%)
S3	982.30 (−42%)	1027.11 (−18%)	1729.68 (−24%)	258.03 (−50%)
S4	2468.77 (+46%)	1491.48 (+20%)	2798.00 (+22%)	865.37 (+69%)
S5	1652.09 (−2%)	647.01 (−48%)	1707.03 (−25%)	360.31 (−30%)

as it was in CTL in the same region. Rear inflow just behind the convective line is only slightly stronger than at the back of the stratiform rain region. This simulation shows that ice processes can result in a noticeable buoyancy gradient and enhancement in the rear-inflow rather far from the convective line itself. Fovell and Ogura (1988) also found that the inclusion of ice extends the scale of the simulated stratiform region. Weisman (1992) concluded from a model lacking ice microphysics that the strength and behavior of the rear-inflow jet was a function of the intensity of the horizontal buoyancy gradients near the back edge of the system. Ice processes alter the buoyancy fields, and therefore modulate the behavior of the circulations (Lafore and Moncrieff 1989). In a system where stratiform region rainfall is much more intense, it is conceivable that the magnitude of the buoyancy gradient and rear-inflow near the rear of the stratiform region might approach that found just behind the convective line.

The increasingly horizontal slope of the rear-inflow jet with time again agrees with observations. The peak magnitude of the jet is about 65% of what it was in CTL at each time, and is therefore much less than observed values. When added to the ambient flow (Fig. 2c), only a weak rear-inflow jet exists in this simulation and it is not horizontally extensive. In addition, in C2, the FTR jet at mid and upper levels is enhanced by less than 50% of what it was in CTL. Convective heating

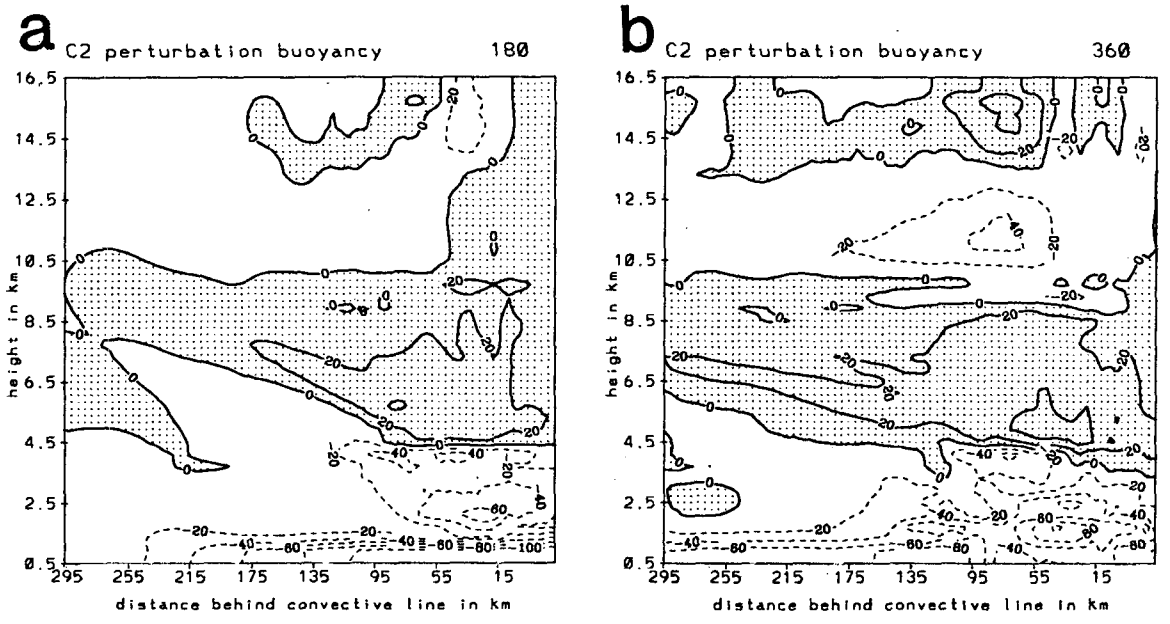

FIG. 9. As in Fig. 4 except for C2, the simulation excluding convective line heating.

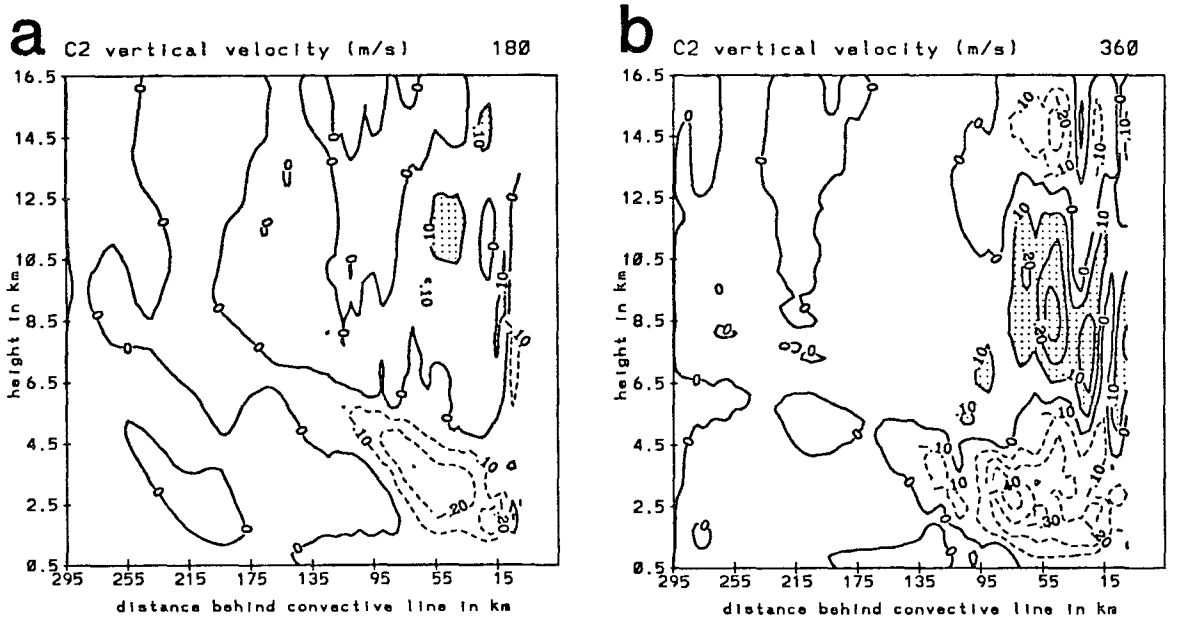

FIG. 10. As in Fig. 5 except for C2, the simulation excluding convective line heating.

therefore must be an important generator of the strong FTR flow found above the rear-inflow jet in the stratiform anvil cloud, as can be seen by comparing the perturbation buoyancy field in CTL (Fig. 4) with that in C2 (Fig. 9).

It is apparent that microphysical processes alone within the stratiform region contribute importantly to the rear-inflow circulation, consistent with Szeto et al. (1988). However, the addition of convective heating is critical to achieve a rear-inflow jet of the intensity observed for the 10–11 June case.

5. Heat advection alone

Another simulation (C3) is run in which the convective line does not supply hydrometeors to the do-

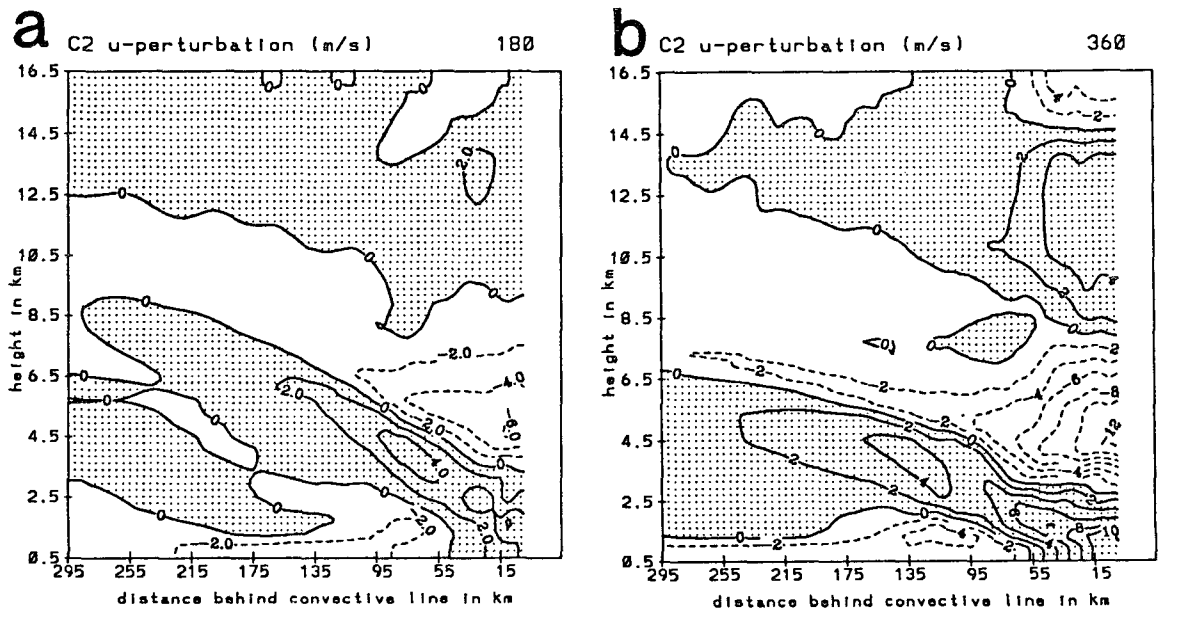

FIG. 11. As in Fig. 6 except for C2, the simulation excluding convective line heating.

main, but does release heat. The strong convective heating induces upward motion in the stratiform domain, which produces some condensate, but the peak snow mixing ratios are less than 50% of the CTL values at all times, and surface rainfall is insignificant (Table 2). Because the in situ production of condensate is rather small, rainfall does not reach the surface until after 315 min, and the peak rain rates are less than 1 mm h^{-1} (figure not shown).

The perturbation buoyancy fields in C3 are primarily different from CTL at low levels (Fig. 12). Without substantial rainfall, negative buoyancy is largely absent in the domain. Horizontal gradients are much weaker, even though positive buoyancy in the anvil cloud is reduced on average by less than 25%.

Peak upward motion within the domain (Fig. 13) is therefore still rather strong, and often similar to that in CTL (Fig. 5), even though rainfall is negligible at the surface. At 180 min (Fig. 13a), the peak upward motion exceeds 40 cm s^{-1}, at least as strong as it is in CTL, but the upward motion is confined to an even smaller region just behind the convective line at around the 6.5-km level. After this time, upward motion exceeding 10 cm s^{-1} spreads rearward nearly 100 km. Upward motion intensifies by 360 min (Fig. 13b) and shows similar patterns to that in CTL. The peak magnitudes, however, remain at 50%–90% of those in CTL, and significant upward motion (exceeding 10 cm s^{-1}) covers smaller regions of the anvil cloud. Ascent is stronger in C3 than in C2, implying a strong dependence on convective heating. The fact that surface precipitation is so small in spite of rather significant upward motion implies the importance of hydrometeor advection and seeder-feeder type processes within the stratiform anvil cloud, as found by Rutledge and Houze (1987). With a kinematic model, that study showed that in cases with the same vertical motion field, the exclusion of rearward hydrometeor advection greatly diminishes surface rainfall. This is true even though a majority of the condensate within the anvil cloud may be produced in situ. Hydrometeors from the convective line are necessary to scavenge the condensate produced in the anvil cloud.

Some important water budget terms for this case are compared with CTL in Table 2. Because mesoscale ascent is greater in C3 than in C2, the production of condensate is also greater. However, rainfall at the surface is greater in C2 than in C3, implying the importance of hydrometeor advection in allowing rainfall to reach the surface in the stratiform region. Both in situ production of condensate and surface rainfall are much larger in CTL than in either C2 or C3, showing that both convective heating and hydrometeor advection are necessary to explain significant stratiform precipitation. The processes that add condensate mass to the hydrometeors from the convective line add substantially to the latent heat release and upward motion in the anvil cloud. Other simulations in which only high-level condensate in the form of ice entering the domain in varying amounts did not reproduce features nearly as similar to those observed as in CTL. Precipitating hydrometeors advected from the convective line are necessary to produce substantial surface rainfall.

Mesoscale descent (Fig. 13) is significantly less in C3 than in CTL since the mesoscale downdraft is so strongly dependent upon evaporation, melting, and

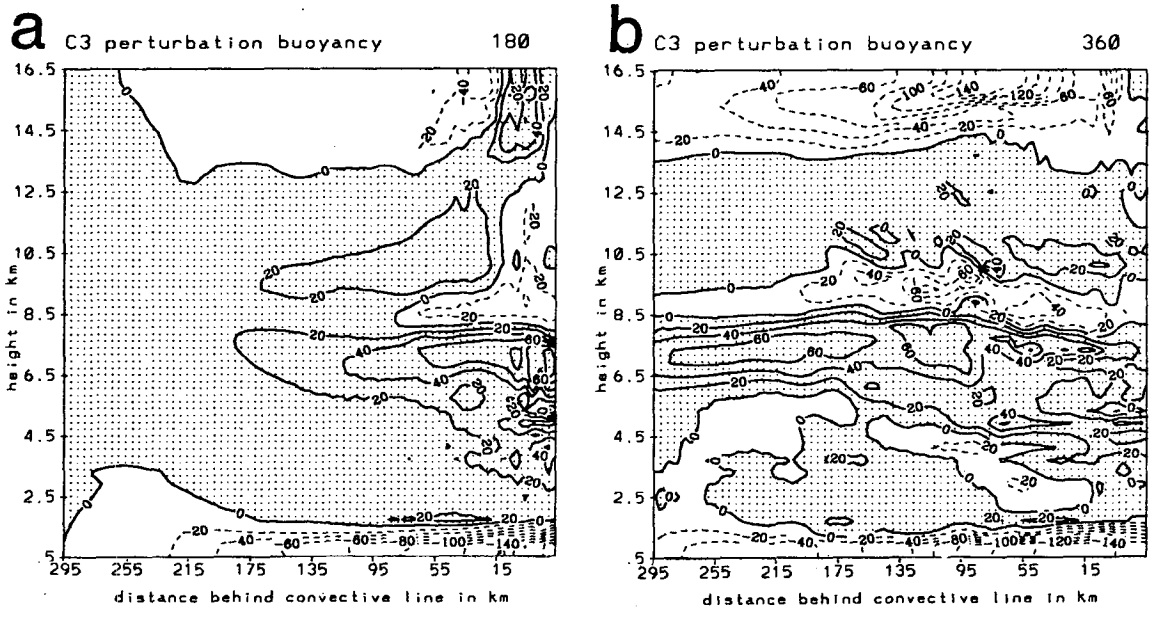

FIG. 12. As in Fig. 4 except for C3, the simulation excluding hydrometeor advection from the convective line.

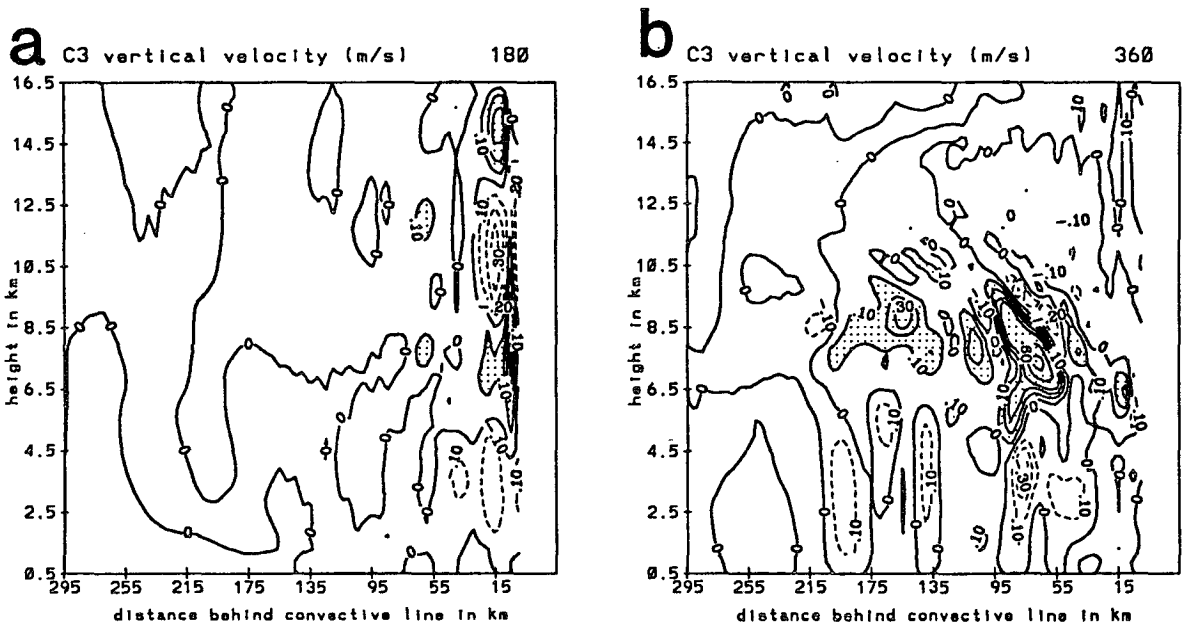

FIG. 13. As in Fig. 5 except for C3, the simulation excluding hydrometeor advection from the convective line.

sublimation of the hydrometeors in the stratiform region. The descent occurs over a much smaller area than in CTL, and the peak value is under 20 cm s^{-1} at 180 min (Fig. 13a), and only exceeds 30 cm s^{-1} after 360 min (Fig. 13b), values less than half those in CTL.

Without strong diabatic cooling processes in the stratiform region in C3, the perturbation horizontal flows (Fig. 14) are significantly different from those in CTL (Fig. 6). Rear inflow does develop at low levels, but the jet does not slope as in CTL. This is supported by Weisman (1992), who found that without a cold pool, the rear-inflow jet remains elevated. Rear inflow is strongest just behind the convective line, but the peak values here are roughly 40%–50% less than in CTL. FTR flow is enhanced in midlevels by the convective heating, but this flow is also reduced by a sim-

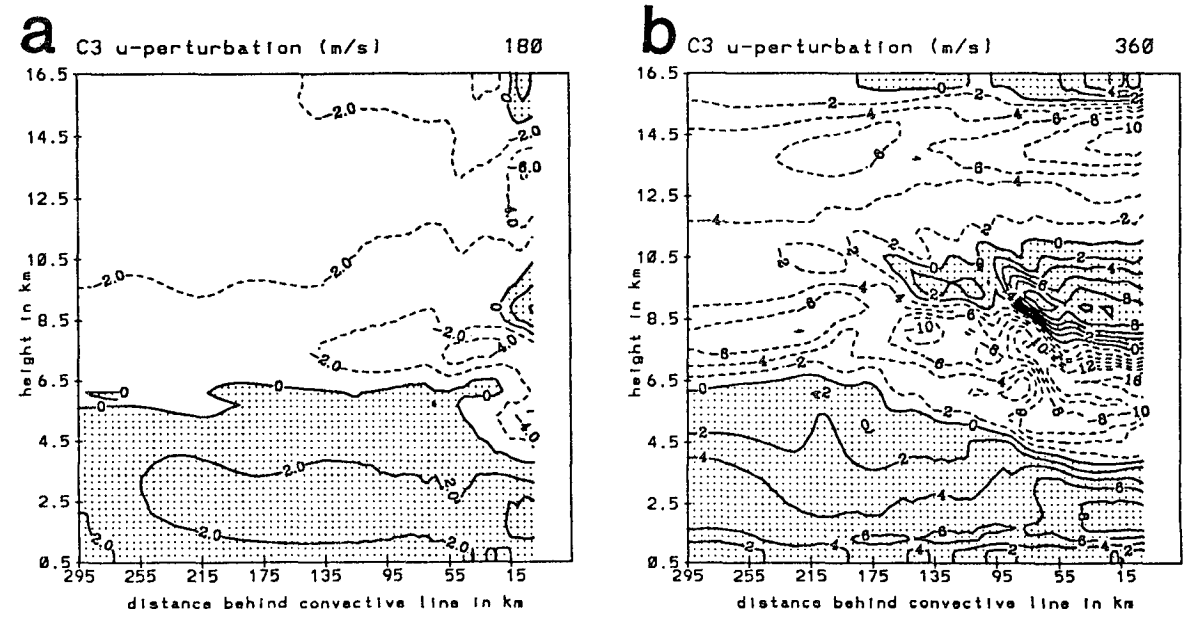

FIG. 14. As in Fig. 6 except for C3, the simulation excluding hydrometeor advection from the convective line.

ilar amount from that in CTL. The diminished horizontal perturbations are due to the weakened buoyancy gradients.

In summary, simulations C2 and C3, together with the CTL simulation, show the importance of both hydrometeor advection and in situ production of condensate, which is strongly related to the convective line heating, in producing broad areas of significant rainfall at the surface, and generating strong horizontal and vertical motions in the stratiform region. Without convective heating, mesoscale ascent is very weak, and although rain does occur over a fairly broad area, the total rainfall is much less than in a simulation where convective heating also plays a role. Convective heating alone, without the advection of hydrometeors, results in almost no surface rainfall, even though in situ generation of condensate is substantial. These results as they relate to surface rainfall support the conclusions of Rutledge and Houze (1987) determined from a kinematic model. The results also elaborate on those earlier findings by showing the importance of hydrometeor advection and convective heating in generating significant circulations.

6. Individual processes

A series of simulations are performed in which one process is neglected as a source or sink of diabatic heating. In these simulations, all processes take place and influence the mixing ratios of hydrometeors and vapor present, but certain processes are excluded from the diabatic heating term. This set of simulations is designed to test the roles of individual processes in developing the circulations that occur in the stratiform region.

In simulation C4, melting is excluded from the diabatic heating term. Although melting is restricted to a narrow layer, it has a significant impact on the buoyancy field by 360 min (Fig. 15a). Prior to this time, the only significant difference between the buoyancy in C4 and CTL was a weakening of the negative perturbation near the melting level. However, positive buoyancy aloft is generally weaker in C4, and at 360 min, the peak positive buoyancy is 20%–30% less than in CTL.

The reduction in buoyancy gradients, especially at midlevels where melting serves to greatly sharpen gradients, results in weaker circulations (Figs. 15b and 15c). The downdraft is especially diminished, due to the exclusion of the cooling from melting (Fig. 15b). Because the downdraft is weaker, rain evaporation, and therefore the mass sink, decreases from CTL (Table 2). In spite of a smaller mass sink, surface precipitation decreases due to the reduction in source terms caused by weaker mesoscale ascent.

Horizontal perturbation flows (Fig. 15c) decrease slightly from the CTL run (Fig. 6b). The rear-inflow jet is similar to that in CTL, but magnitudes are roughly 15% less. The jet descends more gradually, and is especially weaker in the region of heaviest rainfall, not far from the back edge of surface precipitation ($x \approx 135$ km). The FTR flow aloft is slightly weaker, but more substantially differs from CTL near the melting level.

Simulation C4 shows that although melting occurs within a small layer, it has nonnegligible effects on the circulations in the stratiform region. Melting serves to greatly increase convergence near the base of the anvil cloud. This result is supported by Doppler data from tropical oceanic MCSs (Mapes and Houze 1995), which show the strongest convergence in the stratiform region just above the melting level. Leary and Houze (1979) and Szeto et al. (1988), among others, have also shown that melting can have a significant affect on the circulations in the stratiform region.

Simulation C5 excludes evaporative cooling from the diabatic heating. Because evaporation occurs over a larger area than melting, it is understandable that the buoyancy field should change from CTL more than in C4 (Fig. 16a). Most of the negative buoyancy at low levels disappears in C5. Only a small band of negative buoyancy exists near and just above the melting level due to the cooling from sublimation and melting. Positive buoyancy aloft changes less from CTL than in C4.

The lack of negative buoyancy through a deep layer at low levels greatly affects the strength and behavior of the RTF flow. Downward motion is much weaker and less organized than in CTL and C4 (Fig. 16b). The importance of evaporation in forcing a mesoscale downdraft in the stratiform region has also been indicated by Brown (1979) and Zhang and Gao (1989) in numerical modeling studies. Cooling from melting and sublimation, along with rain drag, is able to induce some descent but peak values are roughly half those of CTL. This results in a substantial decrease in the moisture sink term of the water budget (Table 2). The reduction in the sink term more than compensates for a small reduction in the source terms so that surface rainfall increases by over 50%.

The rear-inflow jet itself is significantly different in C5 (Fig. 16c). Most of the RTF perturbation flow occurs within 2–3 km of the surface in a horizontal band, similar to that in the simulation without hydrometeor advection (C3). The FTR flow also decreases, primarily within 100 km of the convective line.

Of processes within the stratiform region, evaporation appears to be the main process contributing to the development and maintenance of a descending rear-inflow jet in the simulations of the 10–11 June system. Simulations C2 and C3 show that the convective line heating plays a comparable role in generating RTF flow, but these results together with those from C5 indicate that it is the evaporation in the stratiform region that drives the rear-inflow jet downward. This is consistent with Weisman (1992), who suggested a descending rear-inflow jet will be forced if there are

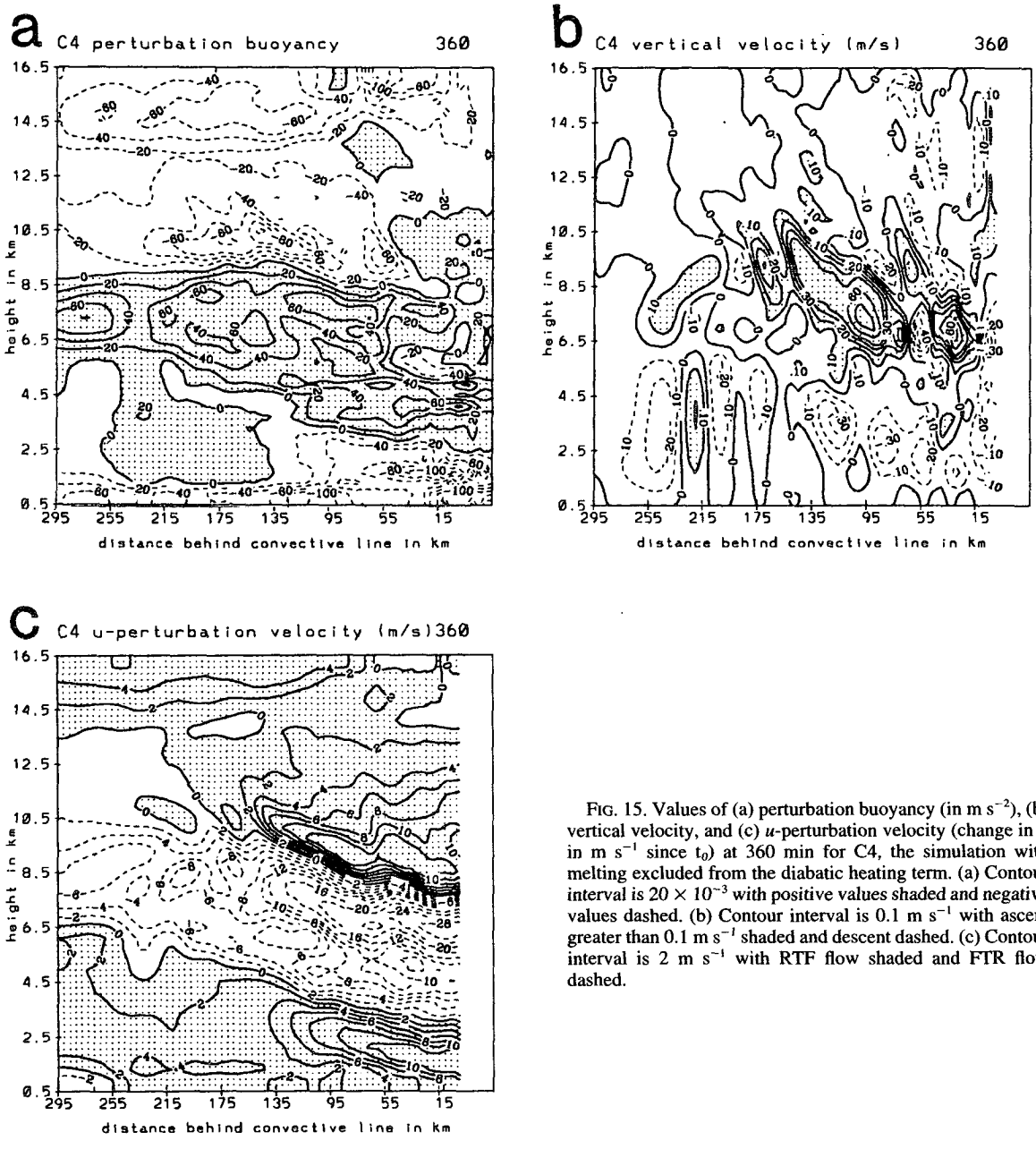

FIG. 15. Values of (a) perturbation buoyancy (in m s^{-2}), (b) vertical velocity, and (c) u-perturbation velocity (change in u in m s^{-1} since t_0) at 360 min for C4, the simulation with melting excluded from the diabatic heating term. (a) Contour interval is 20×10^{-3} with positive values shaded and negative values dashed. (b) Contour interval is 0.1 m s^{-1} with ascent greater than 0.1 m s^{-1} shaded and descent dashed. (c) Contour interval is 2 m s^{-1} with RTF flow shaded and FTR flow dashed.

strong horizontal buoyancy gradients associated with the cold pool near the surface, which is primarily produced by evaporative processes.

In simulation C6, sublimational cooling is excluded from the diabatic heating term. In this simulation, changes from CTL are generally insignificant, and the results will only briefly be discussed. The perturbation buoyancy field exhibits almost no difference from CTL, except at distances greater than 100 km from the convective line region, where the air has not been moistened to ice saturation by vapor advection from the convective region. Negative buoyancy perturbations are reduced slightly in the vicinity of the rear-inflow jet. The rearmost portion of the mesoscale downdraft near and above the melting level also decreases slightly, so that the water sink term in the moisture budget decreases by a small amount (Table 2). Mesoscale ascent and in situ production of condensate are almost unchanged. Surface rainfall increases slightly due to the weakened downdraft.

The exclusion of sublimation has very little effect on the horizontal winds, producing less than a 1 m s^{-1}

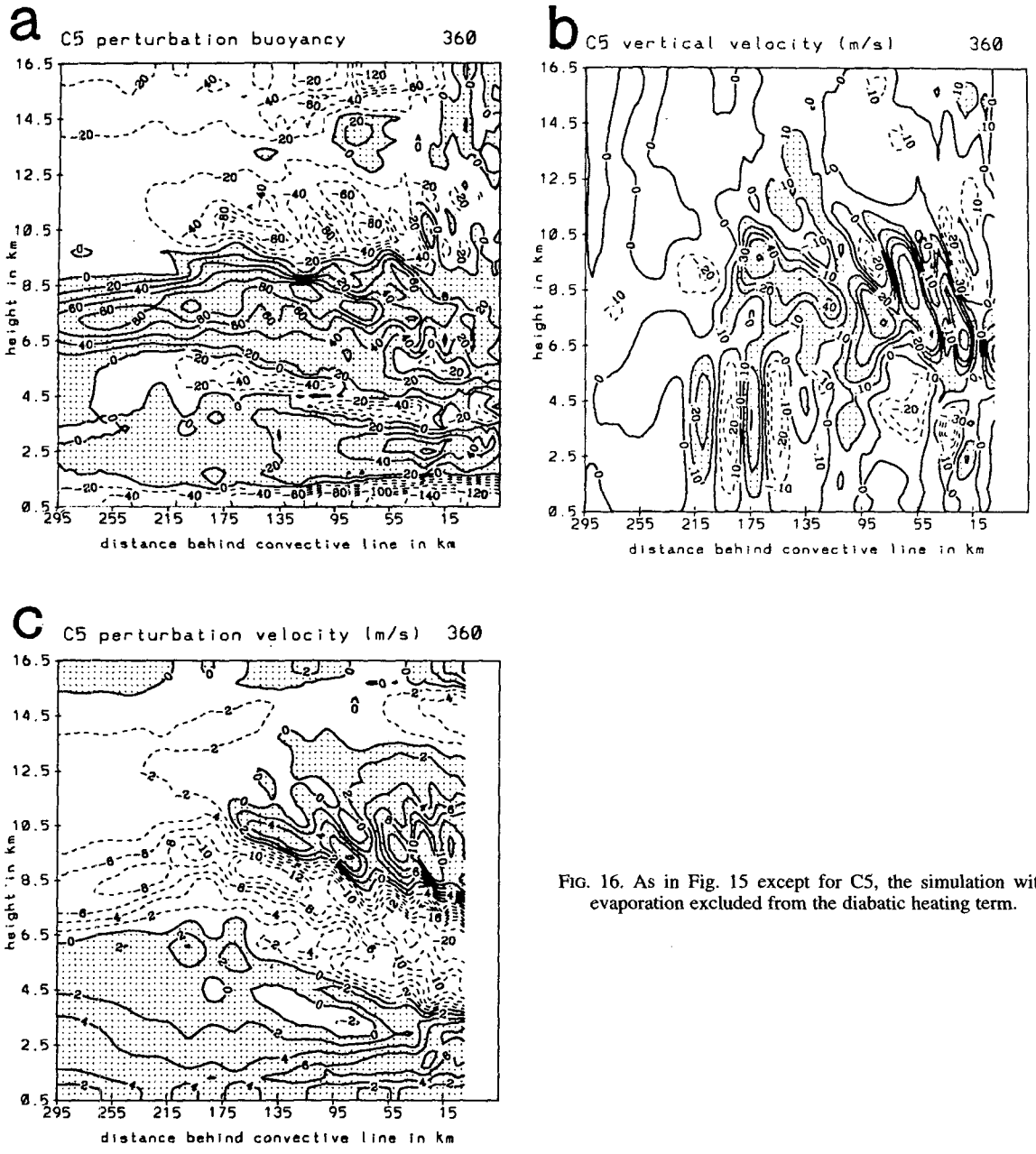

FIG. 16. As in Fig. 15 except for C5, the simulation with evaporation excluded from the diabatic heating term.

decrease in RTF perturbation at most points. In all of the 10–11 June simulations, strong FTR flow advects vapor sufficiently far rearward so that sublimation rates are rather small. Even though downward motion at middle and high levels is more pronounced in the transition zone (Fig. 5) than elsewhere in the domain, sublimation is not a significant factor here, as also found by Braun and Houze (1994). In a subsequent paper, this model will be applied to a different case to show that sublimation can play a much more important role in systems where water vapor is "blocked" from advecting rearward, and hydrometeors are able to pass through regions of relative humidity less than 30% or 40%. The one-dimensional modeling study of Stensrud et al. (1991) also found that sublimation could play a substantial role in generating strong descent in the stratiform region.

In general, these simulations indicate that evaporation of falling rain has the largest effect of any specific microphysical process within the stratiform region on the development of circulations there. (Other simulations were run with the processes of condensation and

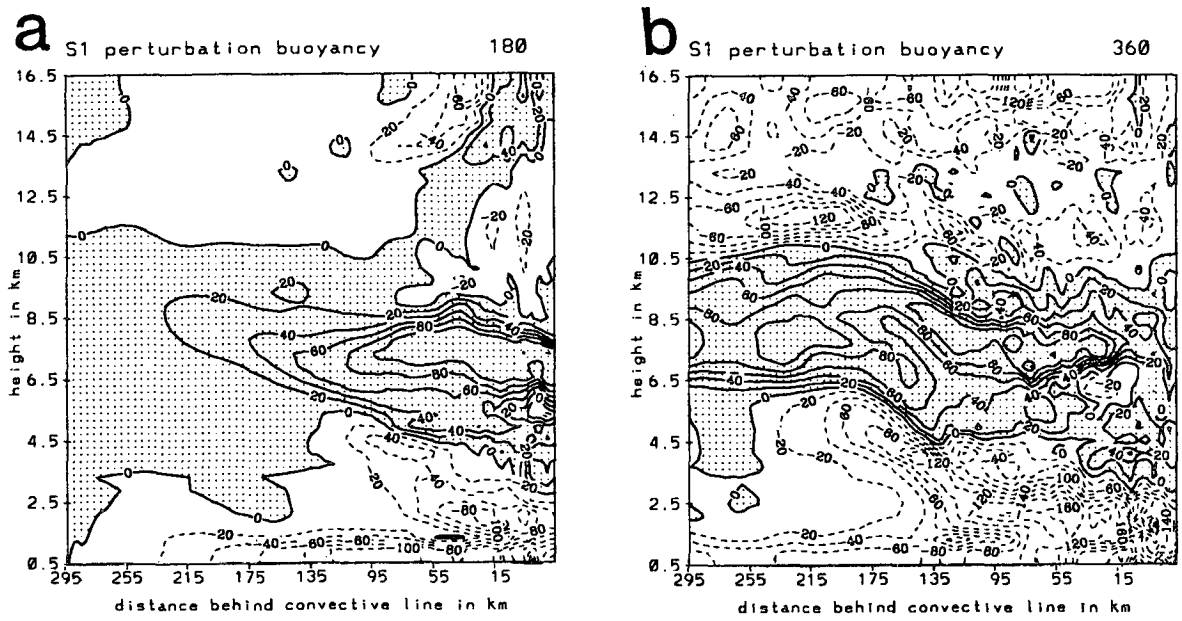

FIG. 17. As in Fig. 4 except for S1, the simulation with increased instability.

vapor deposition isolated, but changes from CTL were small.) Evaporative cooling of at least 1 C h^{-1} occurs over an area that can exceed 100 km, and over a depth of 4 km. No other process heats or cools the atmosphere in the stratiform region over such a broad area through a substantial time interval. These results are supported by the heating budget of the CTL run (Fig. 20; GJ95). The simulations described above also show that heating in the convective line plays the most significant role in creating mesoscale ascent and FTR flow in the trailing anvil. Convective heating also plays a significant direct role in producing strong rear inflow at the front of the stratiform region (Weisman 1992). The convective heating plays a less prominent, indirect role in the evolution of the rear-inflow jet farther to the rear in the stratiform region by increasing the upward motion and in situ condensate production in the anvil cloud. These processes, in turn, increase the amount of microphysical cooling and extend the area influenced by the cooling so that the rear-inflow jet is strengthened farther rearward from the convective line. Even though the convective heating alone is sufficient to generate significant mesoscale ascent in the stratiform region, rearward advection of hydrometeors is necessary to generate significant rainfall over large regions.

7. Sensitivity to environmental conditions

Because the initial conditions used in the CTL run required some interpolation between rawinsondes, and small variations existed in the along-line direction, it is important to investigate the sensitivity of circulations to small changes in the initial conditions. These sensitivity tests also provide possible explanations for the differing behaviors of circulations among different squall line cases. In the simulations, the circulations in the stratiform region were fairly insensitive to small variations in the initial humidity and ambient wind fields. Therefore, emphasis will be given below to the more significant influences by stability, convective cell hydrometeor content, and convective heating.

a. Stability

Soundings from the 11 June system at different times show small variations in stability in the along-line direction. Of all the initial conditions tested, the model is most sensitive to stability variations. Stability is varied in the sensitivity tests within a small range since temperatures at middle and high levels in the stratiform region are fairly uniform. Low-level stability varies more in the observed soundings used for initialization.

Two simulations are run to test model response to lapse rates. In the first, S1, the entire troposphere is assumed to be more unstable, and the lapse rate is increased by 0.6 K km^{-1} at all levels. In the second, S2, the troposphere is made more stable by decreasing the lapse rate by 0.5 K km^{-1}. In both S1 and S2 the temperature at 500 mb is the same as in CTL. Both the temperature profile in S1 and in S2 are in less agreement overall with observations than that used in CTL; however, soundings could be found at certain times within or near the 11 June system that had lapse rates over deep layers more similar to those of S1 and S2 than CTL.

The more unstable environment in S1 results in greater positive buoyancy aloft (Fig. 17) than in CTL

(Fig. 4). This is particularly true at 360 min (Fig. 17b) when peak values exceed 120 × 10^{-3} m s^{-2}, 30% greater than peak values in CTL. Positive buoyancy extends to higher levels in S1 than in CTL. The greater precipitation rates that develop in S1 result in greater negative buoyancy at low levels, so that in some regions, buoyancy gradients are much stronger than in CTL. This is especially evident near the melting level, 135 km rearward of the convective region.

The more unstable environment in S1 leads to markedly stronger vertical motion in the domain with peak ascent (Fig. 18a) nearly doubled from CTL through 180 min (Fig. 5a). Updrafts exceeding 1 m s^{-1} develop shortly after 180 min. The area of strongest ascent continually moves rearward and is generally toward the back of the surface rainfall region. Peak ascent reaches 1.5–2 m s^{-1} at 315 and 360 min (Fig. 18b). The strongest ascent is confined to a rather narrow layer similar to CTL, between 7 and 10 km. The peak values in S1 are somewhat larger than those implied by the rawinsonde study of Gallus and Johnson (1991) and the Doppler study of Rutledge et al. (1988). It therefore appears that although the increased surface rain rates are in better agreement with observations, the cause of the increased rainfall, significantly stronger upward motion in the 7–10-km layer, may not be reasonable. Mesoscale descent is also as much as 50% larger than in CTL.

The intensified vertical motions increase the in situ production of condensate by over 80%, and the water sink by 33% (Table 2). The modeling study of Brown (1979) also found anvil precipitation to be enhanced in more unstable conditions. Snow contents increase by 20%–40% and rain contents underwent similar increases below the melting level (Fig. 19), although a stronger mesoscale downdraft lessens the increase in surface rain rates somewhat. Peak rain rates at the surface are about 1 mm h^{-1} greater than those of CTL at early times (Fig. 19a), but rather intense convective cells form in the anvil cloud after 180 min, greatly enhancing the surface rainfall in small regions. Peak surface values exceed 5 mm h^{-1} consistently after 300 min, peaking at over 10 mm h^{-1} at 360 min (Fig. 19b). These peak values are often more than double those of CTL, not only reaching those observed, but occasionally exceeding them. The average stratiform region surface rain rates in S1 are generally between 1.5 and 2.0 mm h^{-1}. This is an increase of just under 1 mm h^{-1} from the rates in CTL, and the total rainfall at the surface over the simulation is nearly 60% greater than in CTL (Table 2). These rates, however, are still about 1 mm h^{-1} below those observed. Even though isolated areas receive heavier rain, rain is still underestimated over much of the stratiform region.

Consistent with Weisman's (1992) relation of the jet to CAPE (convective available potential energy), horizontal velocity perturbations in S1 increase by 20%–30% with peak RTF exceeding 13 m s^{-1} by 180 min (Fig. 20a), when the peak was only 10 m s^{-1} in CTL (Fig. 6a). The most significant difference between S1 and CTL is in the behavior of the perturbation jets. The RTF jet is much more strongly sloped in S1 during the last half of the simulation, especially at the back of the rain region (Fig. 20b). The difference in slope is greatest at 270 min (figure not shown) when the jet descends 2.5 km over 45 km at the back of the stratiform rain

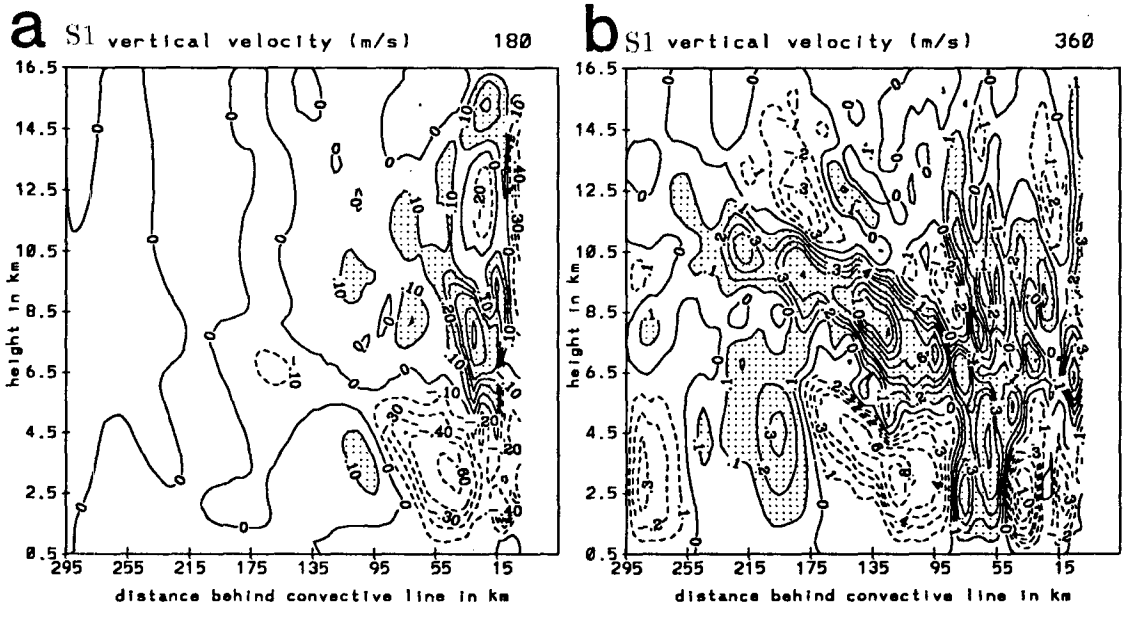

FIG. 18. As in Fig. 5 except for S1, the simulation with increased instability.

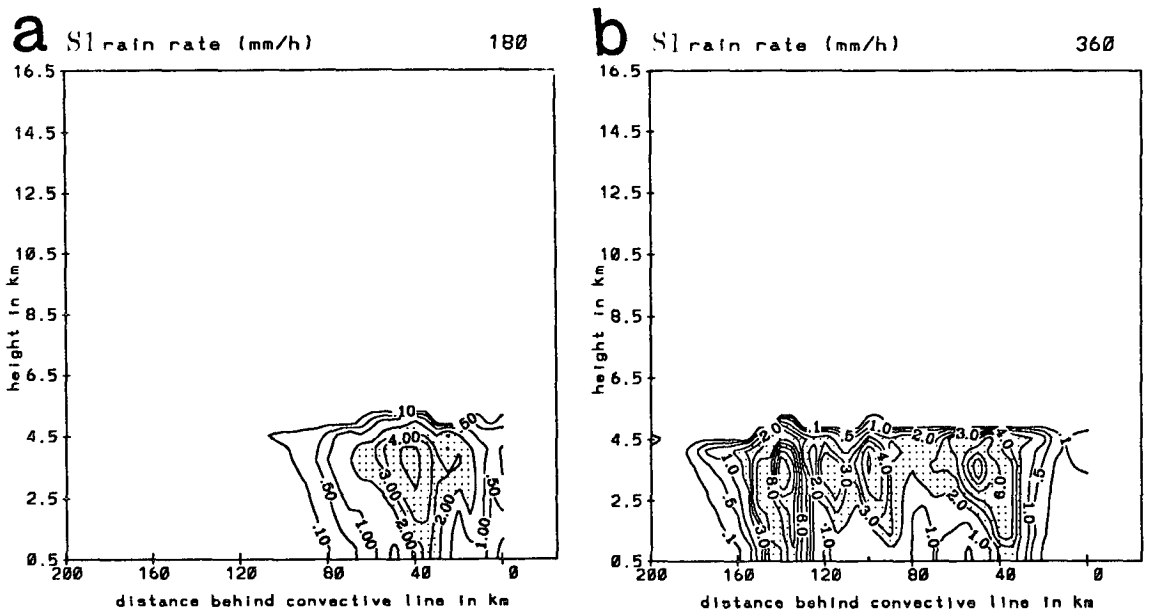

FIG. 19. As in Fig. 3 except for S1, the simulation with increased instability.

region, as opposed to a more gradual 2.0-km descent over 60 km in CTL. The rapid descent of the jet occurs in an area of enhanced buoyancy gradients (Fig. 17b). The RTF flow approaching 10 m s^{-1} can be found 250 km behind the convective line by the end of the simulation, at an elevation of 6.5 km. This is over 100 km rearward of where the same intensities could be found in CTL, and much higher in elevation. Strong FTR flow exists at this location around the 10.5-km level. The FTR flow again is much farther rearward and elevated from positions in CTL.

Some of the features depicted in S1 resemble those in MCS cases where the rear-inflow appears to be blocked and descends abruptly to the surface well behind the convective line (Stumpf et al. 1991). In the 3–4 June case discussed by Stumpf and others, the sud-

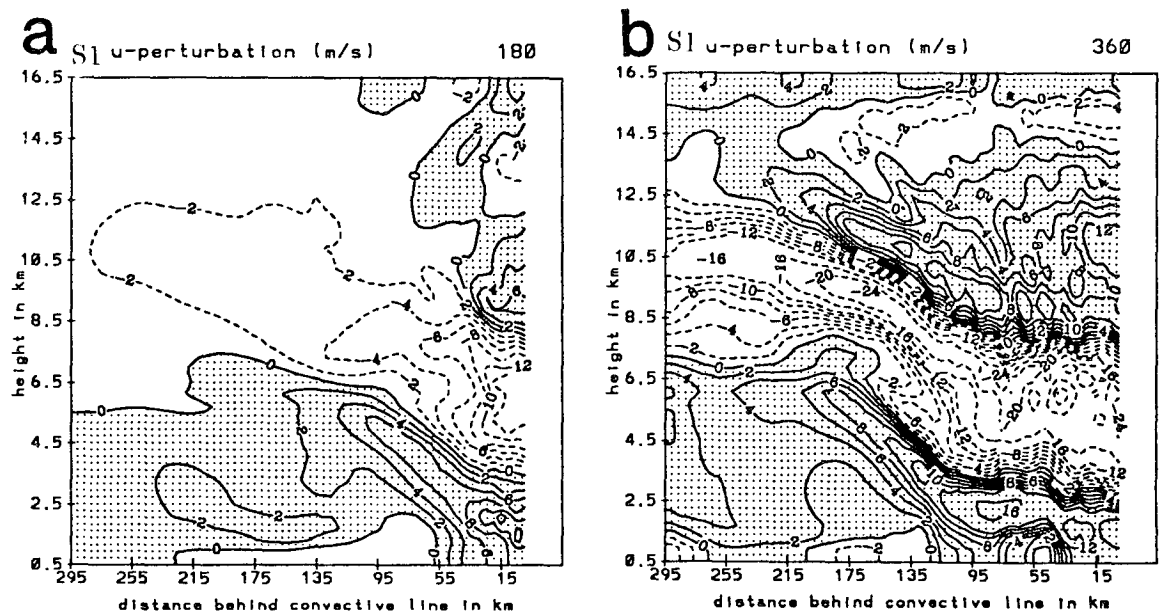

FIG. 20. As in Fig. 6 except for S1, the simulation with increased instability.

den descent of the jet occurred near a region of enhanced reflectivity toward the rear of the stratiform area. In this simulation, the strong ascent, roughly 1.5 m s^{-1} (Fig. 18b) and intense rainfall (Fig. 19b) occur near the back edge of the rain region (around $x = 135$ km). The downdraft here is as large as 1 m s^{-1}. A subsequent paper will discuss the effects of an isolated convective-like cell near the back of the stratiform region on circulations, linking it with the intense downward motion and descent of the rear-inflow jet observed in cases like the 3–4 June PRE-STORM MCS.

The stronger descent in S1 from that in CTL results in more drying at low levels within the stratiform rain region, with humidities decreasing below 50% at isolated locations below the 2.5-km level. Soundings in these areas (Fig. 21) better resemble an onion sounding (Zipser 1977) with its characteristic large T-T_d spread at low levels than any generated in CTL. This particular sounding represents one point near the center of the main rain region at 270 min. This point is in a relative minimum of surface rainfall. The better simulation of an onion sounding may indicate that within the 11 June system, certain areas were more unstable than the region average assumed for CTL. The model results indicate a strong sensitivity to stability. Knupp and Cotton (1987) also found that vertical motions within the stratiform region are rather dependent upon the stability.

Another simulation, S2, is run with a more stable troposphere. As might be expected from the S1 results, vertical motions in this stable simulation are weaker than in CTL with both peak ascent and descent diminished by roughly 20%–30%. This is evidenced by reduced in situ production of condensate (Table 2) and diminished evaporation. The decreases in these terms oppose each other, so that surface rainfall actually increases a small amount. Again, the model displays significant sensitivity to a change in lapse rates, but variations are not as extreme as they are in the more unstable case.

b. *Convective cell hydrometeor content*

The hydrometeor contents used in the 10–11 June squall line simulations are taken from Rickenbach's (1990) values calculated from the Ferrier and Houze (1989) model. These values, varying over 30-min periods as described earlier, are supported by the water budget of Gallus and Johnson (1991), and are therefore reasonably accurate. Two sensitivity tests investigating the model response to hydrometeor content are discussed below. The first test (S3) reduces the snow, ice, and graupel content of the convective cells by 50%. The second test (S4) increases the content by 50%.

A 50% reduction in snow, ice, and graupel entering the domain decreases rain rates in S3 (Table 2). Peak rates aloft are about 40% less than CTL at most times, and the greatest surface rates remain below 1.2 mm h^{-1}

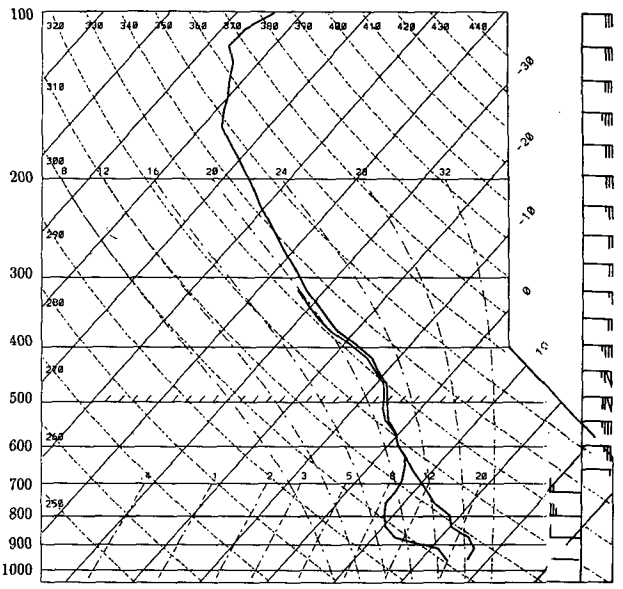

FIG. 21. Thermodynamic diagram from within the stratiform rain region in S1, the simulation with increased instability, at 270 min, with total storm-relative winds shown at the right.

at all times (figure not shown). The relative reduction in total mass of rain reaching the surface during the simulation is rather close to the relative reduction in the mass advecting into the domain.

Perturbation buoyancies are reduced in S3 (Fig. 22a) slightly compared to CTL (Fig. 4b), along with mesoscale ascent (Fig. 22b). In general, the decrease in depositional and condensation heating due to the reduced amount of hydrometeor mass is nearly compensated by the reduced water loading so that the reduction in ascent is small. In fact, prior to 90 min in the simulation, the diminished water loading allows a 30% increase in peak ascent. Mesoscale descent is also diminished, with peak downward motion decreased by roughly 20% at most times (Fig. 22b). The diminished descent also decreases evaporation and sublimation, so that rain rates at the surface are not as low as might be expected from the decrease in both in situ production and advection (Table 2). The decrease in evaporation and sublimation also weakens horizontal perturbation flows.

When hydrometeor advection from the convective line is increased (S4), surface rainfall rates also increase, by an even larger percentage than the increased hydrometeor input (Table 2). Increased hydrometeor advection generates stronger circulations so that nearly 20% more condensate is produced in the stratiform region. The positive feedback of increased hydrometeor advection increasing the in situ production of condensate results in significantly larger surface rainfall in the domain, especially at early times. Peak surface rain rates exceed 3.0 mm h^{-1} at 180 min (Fig. 23a). After this time, increased evaporation results in peak rain

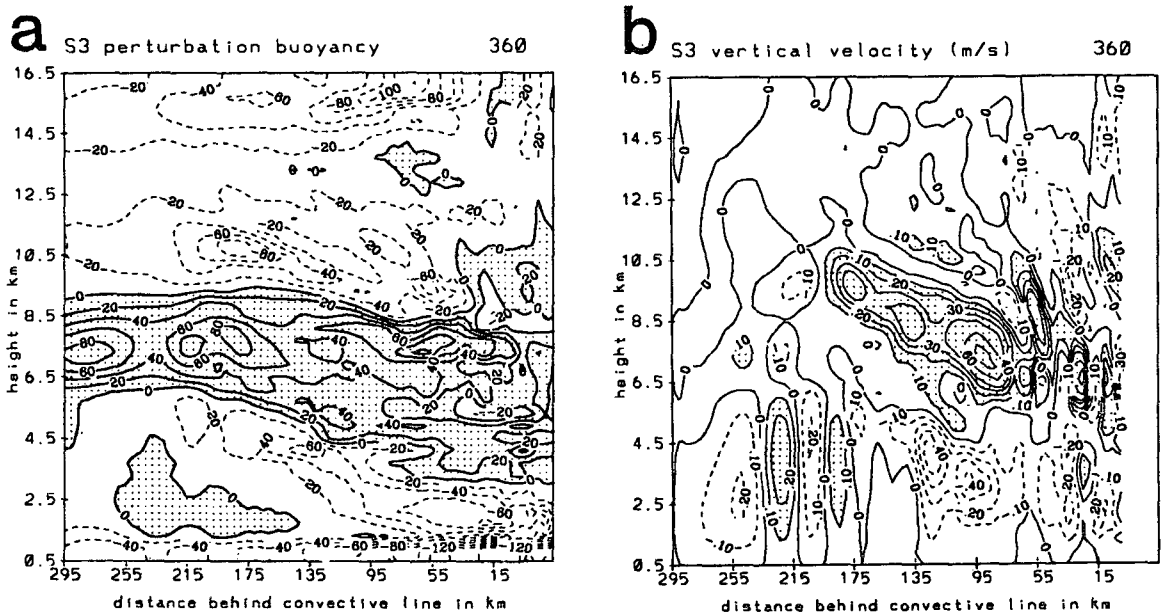

FIG. 22. At 360 min, (a) perturbation buoyancy (in m s^{-2}) and (b) vertical velocity (in m s^{-1}) for S3, the simulation with reduced hydrometeor advection into the domain. Contouring as in Fig. 15.

rates (Fig. 23b) closer to those in CTL (Fig. 3b). Rainfall occurs over a slightly larger area than in CTL, with the transition zone not as wide at later times. Of all the sensitivity tests, the increase of hydrometeors from the convective line causes the greatest amount of rain to reach the surface (Table 2). Peak rainfall generally occurs in the same locations as in CTL, but secondary peaks are more prominent in S4.

Positive perturbation buoyancies are generally greater in S4 than in CTL, although the differences are small at 360 min (Fig. 24a). The negatively buoyant region is similar to that in CTL. During the first 180 min of the simulation, peak upward motion is less than in CTL, probably due to the effects of increased water loading, but peak ascent exceeds that of CTL at later times (Fig. 24b). The increased rain

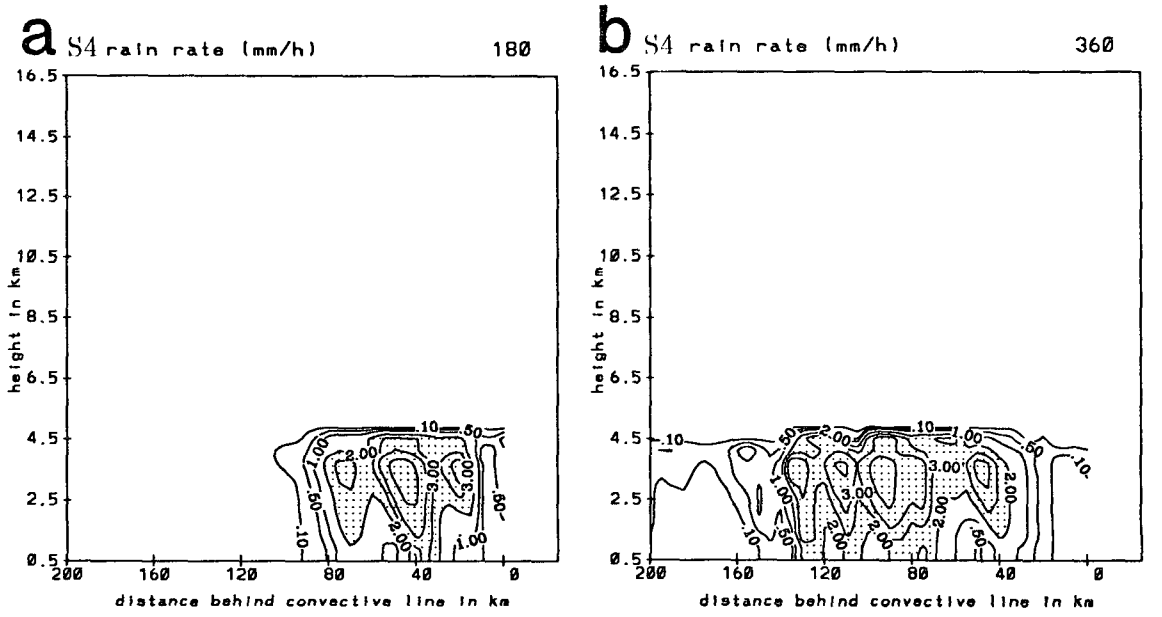

FIG. 23. As in Fig. 3 except for S4, the simulation with increased hydrometeor advection into the domain.

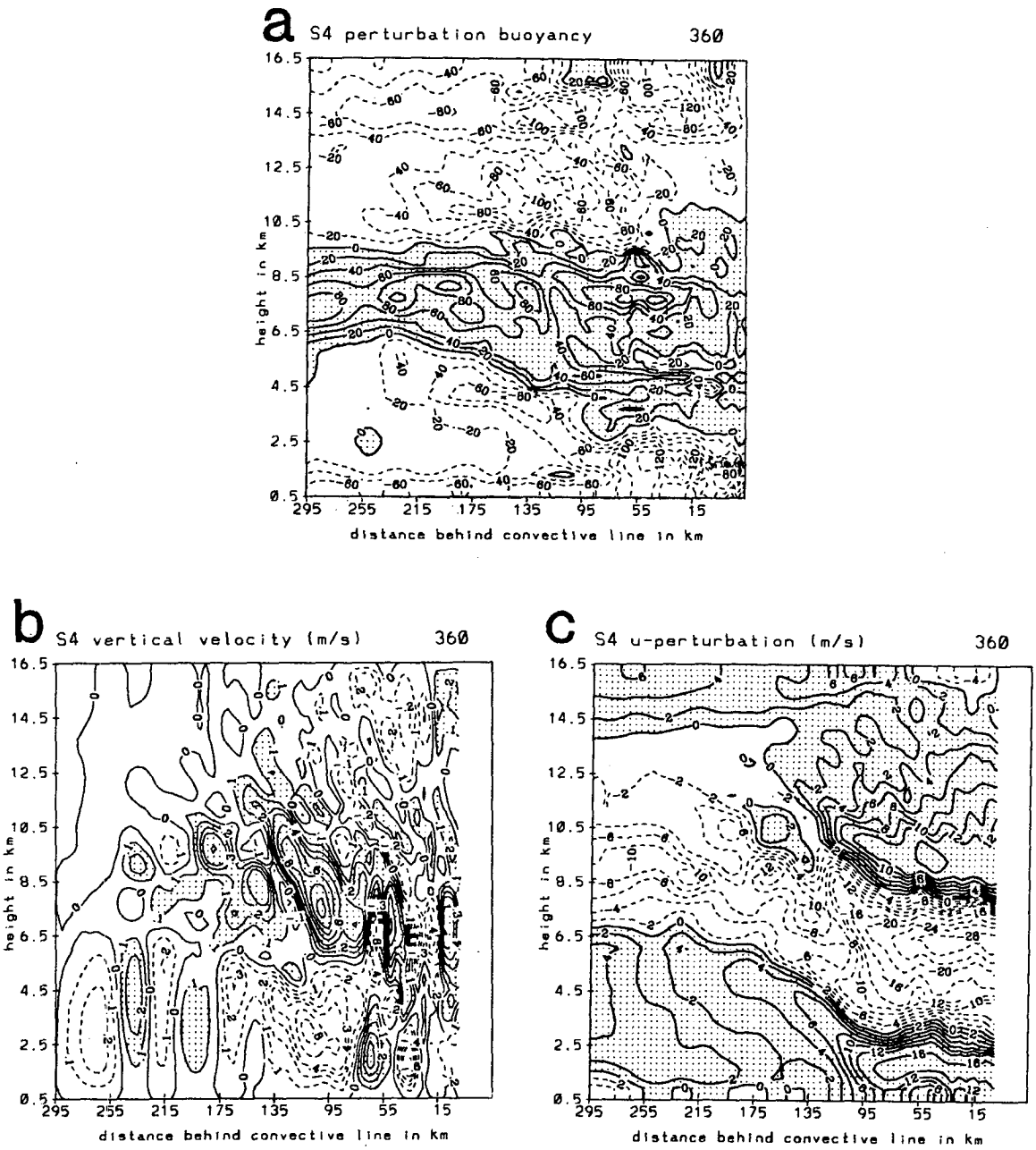

FIG. 24. As in Fig. 15 except for S4. (b) Absolute values greater than 0.4 m s^{-1} are contoured with an interval of 0.2 m s^{-1}. (c) Absolute values greater than 12 m s^{-1} are contoured with an interval of 4 m s^{-1}.

rates enhance evaporation, producing a slightly stronger mesoscale downdraft. Peak values are generally 10%–30% higher at most times, but the locations of vertical motion extrema are similar to those in CTL. The increased evaporation is primarily responsible for a 15% increase in the strength of the peak RTF velocity perturbation (Fig. 24c). The FTR flow increases some rearward of 135 km. The jet axes are sloped similarly in both simulations. The increased surface rainfall (and also low-level reflectivities) in S4 agrees better with mesonet and radar observations of this case (Gallus and Johnson 1991; Rutledge et al. 1988) than CTL. However, the reflectivities near and above the melting level are overestimated in S4, and agree with observations better in CTL and S3. These fields suggest that CTL is as good a simulation of the 10–11 June system as either sensitivity test, and again imply that perhaps the microphysical parameterization overestimates evaporation, as suggested by Ferrier (1994).

In both S3 and S4, the amount of rain reaching the surface in the stratiform region depends highly on the amount of hydrometeor mass advecting rearward from the convective line. A positive feedback exists between the amount of hydrometeors advecting into the region and the amount of condensate produced within the anvil cloud. In fact, changes in surface precipitation (Table 2) are greater for variations in hydrometeor content than for any other sensitivity test examined. This result has significant implications. For instance, it shows that if the convective line is not directly modeled, accurate measurements or estimates of convective cell hydrometeor content may be extremely important for accurate modeling of stratiform regions. This result is supported by Ferrier and Houze (1989). In addition, the intensity of the stratiform region, both from a rainfall and circulation perspective, may depend heavily on the amount of hydrometeors that are advected away from the convective line. This may be a function of the intensity of the convection itself, or the environmental flow in the vicinity of the convective line.

c. *Convective cell heating*

The convective heating prescribed in the buffer zone in the CTL run is based primarily on the 0300 UTC heat budget result for this case by Gallus and Johnson (1991). Sensitivity tests show relatively little change in the circulations when heating is increased as much as 50%–70%. However, when the shape of the heating profile is changed, more significant variations occur in the stratiform region.

Simulation (S5) investigates the influence of the shape of the vertical heating profile in the convective line on circulations in the stratiform region. The peak heating in S5 is equivalent to that in CTL, 12 C h^{-1}, but occurs 2 km higher, around the 8-km level (see Fig. 2b). The shape of the heating profile is changed, so that vertical gradients of heating are diminished in S5. The total amount of heating is greater than in CTL, and is similar to that in a sensitivity test where the CTL heating peak was increased by 5 C h^{-1}. In that sensitivity test, however, changes from CTL were rather small.

The variation of the shape of the convective heating curve causes significant model differences from CTL. Perturbation buoyancies are greatly diminished in S5 from CTL (Fig. 25a), and the field is much smoother, so that forcing is substantially weaker.

Rainfall rates at the surface in general are reduced by 30% from those of CTL (Table 2). The reduced rainfall is due primarily to a nearly 50% decrease in in situ condensate production caused by much weaker ascent aloft (Fig. 25b). Both mesoscale ascent and descent decrease in S5 from CTL with peak ascent never exceeding 30 cm s^{-1}. The ascent occurs rather uniformly through the anvil cloud in a broad region, with much less variation than in CTL (Fig. 5). Mesoscale descent is also diminished, with peak values 10%–40% less than those in CTL. The water sink through evaporation and sublimation is 24% less than in CTL. As would be expected with much weaker vertical motions, the horizontal circulation also diminishes in strength.

The significant decrease in surface rainfall and circulation intensity in S5 has ramifications for other modeling studies in which a heating profile is prescribed to represent the convective line of a squall line system. Even though the peak heating in S5 is the same as in CTL, and the total heating through the depth of the troposphere is actually larger than in CTL, the dynamics of the stratiform region resembled those of C2, the simulation without convective heating more than those of the runs with the CTL heating profile. The effects of convective heating may be underestimated if vertical gradients of heating are overly smoothed. Fortunately, the profile used in the CTL case is supported by the 0300 UTC heat budget of Gallus and Johnson (1991), which showed rather strong vertical gradients of convective heating. The rain rates and vertical motions that occur in CTL are also in closer agreement with those observed on 11 June.

8. Conclusions and discussion

A two-dimensional anelastic mesoscale cloud model, with a detailed bulk microphysical parameterization (Rutledge and Hobbs 1983, 1984), is used to investigate the interaction between the convective line and stratiform regions of the 10–11 June PRE-STORM squall line. The role of individual microphysical processes and initial conditions in the development of circulations in the stratiform region is also investigated. Simulations are run isolating the effects of hydrometeor advection from the convective line and convective heating itself. Variations are made in the stability of the environment and in the hydrometeor contents and shape of the heating profile within convective line elements. Comparisons are made with a control simulation of the 10–11 June PRE-STORM case (GJ95).

In the absence of convective heating, hydrometeor advection alone into the stratiform region does induce mesoscale ascent with some in situ production of condensate. However, circulations are much weaker than those present with convective heating, and surface rainfall is reduced by roughly 40%. Convective heating without hydrometeor advection induces stronger circulations and greater in situ production of condensate, but little, if any, surface rainfall. Hydrometeors from the convective line are necessary to scavenge the condensate.

In general, accumulated surface rainfall is relatively insensitive to many variations in initial conditions since the same factors that increase the in situ production of condensate also increase the strength of the mesoscale downdraft and the associated water sink. Stability of the postconvective line environment greatly influences

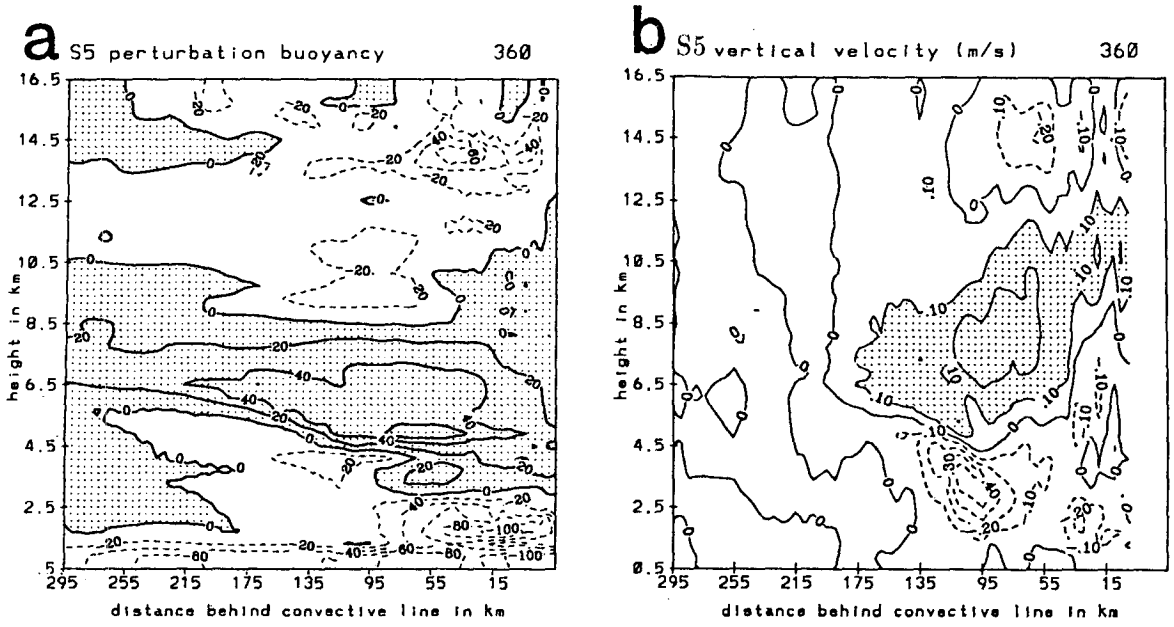

FIG. 25. Values of (a) perturbation buoyancy (in m s^{-2}) and (b) vertical velocity (in m s^{-1}) at 360 min for S5, the simulation with an altered convective heating profile. (a) Contour interval is 20×10^{-3} with positive values shaded and negative values dashed. (b) Contour interval is 0.1 m s^{-1} with ascent greater than 0.1 m s^{-1} shaded and descent dashed.

the behavior of the stratiform region, with small increases in instability manifesting themselves as large increases in vertical motion and production and destruction of condensate. Increased instability also increases surface rainfall significantly. The stronger mesoscale downdraft in a more unstable environment increases low-level drying, producing "onion" soundings (Zipser 1977) that more closely match those observed. Decreased instability weakens vertical motion and in situ production of condensate.

Surface rainfall in the stratiform region is also strongly dependent on the amount of hydrometeors advecting into the domain. A positive feedback occurs so that increased hydrometeor advection results in an increase in the in situ production of condensate and much larger surface rainfall rates. Accurate profiles of convective cell hydrometeor contents may therefore be necessary for simulations of the stratiform region.

The strong sensitivity to both hydrometeor advection and tropospheric stability indicated by the model suggests that these variations may explain some of the three dimensionality seen in the stratiform region. The model is limited by its inability to simulate the feedback of the stratiform region on the convective line, and therefore on the inputs prescribed from the convective line. The simulations are therefore somewhat dependent upon the assumed temporal behavior of the convective line inputs. However, the model response to the variations in stability and hydrometeor content strongly suggest that the heaviest stratiform rain should occur rearward of the strongest convective elements. Of course, along-line flow can serve to weaken this effect. The most intense low-level descent and ascent aloft may occur in regions that are more unstable, either due to variations in ambient stability, or to small variations in the effects convective cells have had on the atmosphere behind them. Because the motions in the stratiform region are significantly affected by the profile of convective heating and the amount of hydrometeors advected rearward, forecasting of these squall line events with larger meshed models will be highly dependent on the accuracy of the cumulus parameterizations used.

Acknowledgments. The authors would like to thank Profs. Steven Rutledge and Wayne Schubert for their assistance in the research. The constructive comments of Dr. Brad Ferrier and two anonymous reviewers significantly improved the manuscript. This research has been supported by a National Science Foundation Graduate Fellowship and National Science Foundation Grant ATM9013112, and completion of the manuscript was possible under the UCAR visiting scientist program at the National Meteorological Center.

REFERENCES

Biggerstaff, M. I., and R. A. Houze Jr., 1991: Kinematic and precipitation structure of the 10–11 June 1985 squall line. *Mon. Wea. Rev.*, **119,** 3034–3065.

Braun, S. A., and R. A. Houze Jr., 1994: The transition zone and secondary maximum of radar reflectivity behind a midlatitude squall line: Results retrieved from Doppler radar data. *J. Atmos. Sci.*, **51,** 2733–2755.

Brown, J. M., 1979: Mesoscale unsaturated downdrafts driven by rainfall evaporation: A numerical study. *J. Atmos. Sci.*, **36,** 313–338.

Ferrier, B. S., 1994: A double-moment multiple-phase four-class bulk ice scheme. Part I: Description. *J. Atmos. Sci.*, **51,** 249–280.

——, and R. A. Houze Jr., 1989: One-dimensional time-dependent modeling of GATE cumulonimbus convection. *J. Atmos. Sci.*, **46,** 330–352.

Fovell, R. G., and Y. Ogura, 1988: Numerical simulations of a midlatitude squall line in two dimensions. *J. Atmos. Sci.*, **45,** 3846–3879.

Gallus, W. A., Jr., and R. H. Johnson, 1991: Heat and moisture budgets of an intense midlatitude squall line. *J. Atmos. Sci.*, **48,** 122–146.

——, and ——, 1992: The momentum budget of an intense midlatitude squall line. *J. Atmos. Sci.*, **49,** 422–450.

——, and ——, 1995: The dynamics of circulations within the stratiform regions of squall lines. Part I: The 10–11 June PRESTORM system. *J. Atmos. Sci.*, **52,** 2161–2187.

Gao, K., D.-L. Zhang, M. W. Moncrieff, and H.-R. Cho, 1990: Mesoscale momentum budget in a midlatitude squall line: A numerical case study. *Mon. Wea. Rev.*, **118,** 1011–1028.

Heymsfield, A. J., and M. R. Hjemfelt, 1984: Processes of hydrometeor development in Oklahoma convective clouds. *J. Atmos. Sci.*, **41,** 2811–2835.

Johnson, R. H., and P. J. Hamilton, 1988: The relationship of surface pressure features to the precipitation and air flow structure of an intense midlatitude squall line. *Mon. Wea. Rev.*, **116,** 1444–1472.

Knupp, K. R., and W. R. Cotton, 1987: Internal structure of a small mesoscale convective system. *Mon. Wea. Rev.*, **115,** 629–645.

Lafore, J., and M. W. Moncrieff, 1989: A numerical investigation of the organization and interaction of the convective and stratiform regions of tropical squall lines. *J. Atmos. Sci.*, **46,** 521–544.

Leary, C. A., and R. A. Houze Jr., 1979: Melting and evaporation of hydrometeors in precipitation from the anvil clouds of deep tropical convection. *J. Atmos. Sci.*, **36,** 669–679.

Mapes, B. E., and R. A. Houze Jr., 1995: Diabatic divergence profiles in western Pacific mesoscale convective systems. *J. Atmos. Sci.*, **52,** 1807–1828.

Ogura, Y., and M.-T. Liou, 1980: The structure of a midlatitude squall line: A case study. *J. Atmos. Sci.*, **37,** 553–567.

Orlanski, I., 1976: A simple boundary condition for unbounded hyperbolic flows. *J. Comput. Phys.*, **21,** 251–269.

Rickenbach, T. M., 1990: Precipitation processes and water budget study of the 10–11 June 1985 mesoscale convective system. M. S. thesis, Colorado State University, 180 pp. [Available from Atmos. Sci. Dept., Colorado State University, Ft. Collins, CO 80523.]

Rotunno, R., J. B. Klemp, and M. L. Weisman, 1988: A theory for strong, long-lived squall lines. *J. Atmos. Sci.*, **45,** 463–485.

Rutledge, S. A., 1986: A diagnostic numerical study of the stratiform region associated with a tropical squall line. *J. Atmos. Sci.*, **43,** 1337–1358.

——, and P. V. Hobbs, 1983: The mesoscale and microscale structure and organization of clouds and precipitation in midlatitude cyclones. VIII: A model for the "Seeder-Feeder" process in warm-frontal rainbands. *J. Atmos. Sci.*, **40,** 1185–1206.

——, and ——, 1984: The mesoscale and microscale structure and organization of clouds and precipitation in midlatitude cyclones. XII: A diagnostic modeling study of precipitation development in narrow cold-frontal rainbands. *J. Atmos. Sci.*, **41,** 2949–2972.

——, and R. A. Houze Jr. 1987: A diagnostic modeling study of the trailing stratiform region of a midlatitude squall line. *J. Atmos. Sci.*, **44,** 2640–2656.

——, ——, M. I. Biggerstaff, and T. Matejka, 1988: The Oklahoma–Kansas mesoscale convective system of 10–11 June 1985: Precipitation structure and single-Doppler radar analysis. *Mon. Wea. Rev.*, **116,** 1409–1430.

Smull, B. F., and R. A. Houze Jr., 1985: A midlatitude squall line with a trailing region of stratiform rain: Radar and satellite observations. *Mon. Wea. Rev.*, **113,** 117–133.

——, and ——, 1987: Rear inflow in squall lines with trailing stratiform precipitation. *Mon. Wea. Rev.*, **115,** 2869–2889.

Stensrud, D. J., R. A. Maddox, and C. L. Ziegler, 1991: A sublimation-initiated mesoscale downdraft and its relation to the wind field below a precipitating anvil cloud. *Mon. Wea. Rev.*, **119,** 2124–2139.

Stumpf, G. J., R. H. Johnson, and B. F. Smull, 1991: The wake low in a midlatitude mesoscale convective system having complex convective organization. *Mon. Wea. Rev.*, **119,** 134–158.

Szeto, K. K., C. A. Lin, and R. E. Stewart, 1988: Mesoscale circulations forced by melting snow. Part I: Basic simulations and dynamics. *J. Atmos. Sci.*, **45,** 1629–1641.

Weisman, M. L., 1992: The role of convectively generated rear-inflow jets in the evolution of long-lived meso-convective systems. *J. Atmos. Sci.*, **49,** 1826–1847.

Zhang, D.-L., and K. Gao, 1989: Numerical simulation of an intense squall line during 10–11 June 1985 PRE-STORM. Part II: Rear inflow, surface pressure perturbations, and stratiform precipitation. *Mon. Wea. Rev.*, **117,** 2067–2094.

Zipser, E. J., 1977: Mesoscale and convective-scale downdrafts as distinct components of squall-line structure. *Mon. Wea. Rev.*, **105,** 1568–1589.